Discovery of re-purposed drugs that slow SARS-CoV-2 replication in human cells

*Adam Pickard, Ben C. Calverley, Joan Chang, Richa Garva, Yinhui Lu, and *Karl E. Kadler

Wellcome Centre for Cell-Matrix Research, Faculty of Biology, Medicine & Health, University of Manchester, Manchester Academic Health Science Centre, Manchester, M13 9PT UK

* Co-corresponding authors: AP email: adam.pickard@manchester.ac.uk (orcid.org/0000-0001-9757-143X); KEK email: karl.kadler@manchester.ac.uk (orcid.org/0000-0003-4977-4683)

Keywords: aliskiren; vitamin D3; ebastine; LY2835219; abemaciclib; panobinostat; manidipine; atovaquone; bedaquiline; amodiaquine; litholicholic acid; NanoLuciferase; screen, bioluminescence; COVID-19; COVID

Open Access

Summary

Background

The SARS-CoV-2 virus has caused the death of over 2 million people worldwide during the COVID-19 pandemic. Whilst effective vaccines have been developed and vaccination schedules are being rolled out, the identification of safe and inexpensive drugs to slow the replication of SARS-CoV-2 could help thousands of people worldwide whilst awaiting vaccination.

Methods

Using SARS-CoV-2 tagged with nano-luciferase (SARS-CoV-2-ΔOrf7a-NLuc) we screened a variety of cells under optimised cell culture conditions for their ability to be infected by, and support the replication of, SARS-CoV-2. Electron microscopy was used to demonstrate generation of infectious virus particles. We assessed a library of 1971 FDA-approved drugs for their ability to inhibit or enhance viral replication in Vero (simian kidney cells) but also in the human hepatocyte cell, HUH7. Initial hits were further tested to identify compounds that could suppress viral replication, post-viral infection. Dose response curves were obtained for a shortlist of 9 compounds of interest (COI).

Findings

Our SARS-CoV-2-ΔOrf7a-NLuc virus was as effective as wild-type SARS-CoV-2 in inducing CPE and replicating in Vero cells. Conventional electron microscopy showed the NLuc-tagged virus to be structurally indistinguishable from the wild-type virus, and both could be identified within the endosomal system of infected cells. SARS-CoV-2-ΔOrf7a-NLuc was used in experiments to robustly quantitate virus infection and replication. A wide variety of human cells including lung fibroblasts and epithelial cells were susceptible to infection but were not effective in supporting SARS-CoV-2-ΔOrf7a-NLuc replication. In contrast, human kidney epithelial cells and human hepatic cells were particularly susceptible and supported SARS-CoV-2-replication, which is in-line with reported proteinuria and liver damage in patients with COVID-19. Our screening of FDA approved compounds identified 35 COI that inhibited virus infection and replication in either Vero or human cell lines. Nine of these also inhibited SARS-CoV-2 replication when treatment commenced after virus infection. Therapeutics approved for treatment of cancer, malaria, hypertension and viral infection were identified with atovaquone, manidipine, vitamin D3 and ebastine being well tolerated with minimal side effects. Only two COI were consistently found to enhance SARS-CoV-2 replication, aliskiren and lithocholic acid.

Interpretation

Re-purposing of safe, well-tolerated FDA-approved drugs that inhibit SARS-CoV-2 replication is an attractive strategy to reduce the risk of COVID-19 infection prior to receiving an effective vaccine. The COI identified here hold potential to contain COVID-19 whilst wide-scale vaccination proceeds. The identification of FDA-approved

drugs that enhance SARS-CoV-2 replication in human cells suggests that entry routes into cells can be made more accessible to the virus by certain medications.

The information provided in this research paper is for information only and is not meant to be a substitute for advice provided by a doctor or other qualified health care professional.

Funding

The research was funded by a grant from the Wellcome Trust (110126/Z/15/Z) to KEK. The Cat 3 facilities were made possible by an award from the BBSRC (BB/T00083X/1) to Jennifer Cavet.

Introduction

The COVID-19 pandemic, caused by the severe acute respiratory syndrome coronavirus 2 (SARS-CoV-2) virus, has had an unprecedented widespread impact on global health with substantial loss of life. The virus enters hosts cells via angiotensin-converting enzyme 2 (ACE2) on the surface of host cells [1]. Academic and pharmaceutical sectors have been quick to respond to the need for effective vaccines aimed at stemming the spread of the virus, and the rollout of vaccinations is currently progressing at pace, especially in developed countries. However, large proportions of the world's population remain at risk of contracting COVID-19 as they wait to be vaccinated, which has prompted governments around the world to encourage people to continue to self-isolate, remain at home, and maintain physical distancing. The identification of safe, cheap, and easily distributed medications that can reduce the risk of death from SARS-CoV-2 infection, would have a significant impact on saving lives and aid the recovery of economies.

The Food and Drug Administration (FDA) and the European Medicines Agency (EMA) work with pharmaceutical companies to develop safe and effective drugs for the benefit of public health. Some FDA-approved drugs whose use is no longer protected by patents have been made available for research use. One of these collections, the APExBIO DiscoveryProbe library of 1971 compounds was used here to identify safe, approved drugs that could inhibit the infection and replication of the SARS-CoV-2 virus in human cells.

We had previously developed an approach to quantitate collagen synthesis by using CRISPR-Cas9 to insert the gene encoding NanoLuciferase (NLuc) into the Col1a2 gene in fibroblasts [2]. Here, we adapted the approach to tag the SARS-CoV-2 virus with NLuc, and then used the recombinant NLuc-tagged virus to screen the APExBIO library of compounds. To draw reliable conclusions from our studies we evaluated a panel of human cell types for their ability to be infected by SARS-CoV-2 and to support virus replication. We evaluated and optimised culture conditions for each cell type to provide a robust method of validation. We found that hepatocytes and kidney epithelial cells were proficient in supporting SARS-CoV-2 replication whereas fibroblasts and lung epithelial cells were less effective. Among the short list of drugs that were effective in inhibiting SARS-CoV-2 replication were anti-cancer, and anti-viral drugs as well as drugs being studied to treat COVID-19. Our screen identified drugs, such as aliskiren and lithocholic acid, that enhanced SARS-CoV-2 replication in cells.

Methods

Cell culture

Cell lines maintained in growth medium are shown in Supplementary Table 1.

Generation of functional SARS-CoV-2 virus

DNA encoding the genome of SARS-CoV-2 and SARS-CoV-2-ΔOrf7a-NLuc were purchased from Vectorbuilder Inc. (Chicago, US). Transfection of virus encoding the DNA failed to generate replicative virus when electroporated into 293T cells. We therefore produced RNA molecules which encoded the virus *in vitro.* Briefly, virus encoding DNA (1 µg) was transcribed using T7 mMessenger mMachine (Thermo) with a GTP:Cap ratio of 2:1 used in a 20 µL reaction. In addition, RNA encoding the SARS-CoV-2 nucleocapsid was also generated by PCR using primers P1 and P2 (Supplementary Table 2). It has been reported that this aids the recovery of replicative virus (Insert ref 3). Viral RNA genomes (10 µl) and 2.5 µL nucleocapsid RNA were

electroporated into 293T cells. Viral RNAs were electroporated (5,000,000 cells, 1100 V, 20 ms and 2 pulses) and grown in T75 cm^2 flasks and 24 well plates. Cells grown in 24 well plates for 24-120 hrs were used to monitor changes in NLuc activity.

Virus production, maintenance and assessment of titre

Culture medium was collected from 293T cells 6 days after electroporation. This virus (P0) was used to infect cells of interest. As virus replication was slow in 293T cells, virus stocks were maintained by passage in Vero cells grown in DMEM supplemented with 2% FBS. Medium (1 mL) was used to infect Vero cells in order to generate P1 virus. Replication was assessed by measuring NLuc activity over 10 days. For subsequent passage of the virus, Vero cells in T75 cm^2 flasks were infected with 2 mL of medium containing virus, after 3 days the medium was collected and passed through 0.45 µm filters using Luer-loc syringes.

To titre the virus, 200,000 Vero cells were seeded in 6-well plates overnight in growth medium. After removing growth medium Vero cells were infected with 200 µL of serially diluted virus containing medium at 37 °C. After 1 hour, wells were overlaid with 2 mL of 0.3% low melt agarose in 2xDMEM containing 1% FBS and grown for 3 days. After 3 days infected cells were fixed with 10% PFA overnight and then stained with crystal violet. Plaques were identified by imaging plates on BioDoc-It gel documentation system (UVP, Upland, US).

To detect viral RNA in medium, 0.25 mL of virus containing medium was collected 3 days post infection, 0.75 mL TriPure LS reagent (Sigma-Aldrich St. Louis, US) was added and RNA isolated according to the manufacturer's recommendations, in the final step RNA was dissolved in 15 µL DNAse/RNAse free water. For detection of SARS-COV-2 nucleocapsid transcripts in lung epithelial cells, 200,000 cells were infected at the indicated MOI for 3 days, monolayers were lysed directly in 1 mL Trizol (Invitrogen, Paisley UK). For assessing expression of ACE2, TMPRSS2 and NLP1 expression in lung epithelial cells RNA was isolated from the cells using Trizol and RNA isolated according to the manufacturer's recommendations. For cDNA generation and real-time PCR we used conditions previously described [3] using primers detailed in Supplementary Table 2.

Electron microscopy

After 3 days infection with P4 virus, Vero cells were scrapped and pelleted. Cell pellets were fixed using 2.5% glutaraldehyde and 4% paraformaldehyde in 0.1 M cacodylate buffer for 24 h, washed in ddH_2O three times, 30 mins for each wash. Cell pellets were incubated in freshly made 2% (vol/vol) osmium tetroxide and 1.5% (wt/vol) potassium ferrocyanide in cacodylate buffer (100 mM, pH 7.2) for 1 hr at room temperature. Samples were washed in ddH_20 five times each for 3 minutes. Specimens were transferred to freshly made 1% (wt/vol) tannic acid in 100 mM cacodylate buffer (pH 7.2) for 40 mins at RT and washed in ddH_2O five times for 3 mins each at RT. The specimen was incubated with 1% (vol/vol) osmium tetroxide in ddH_2O for 30 minutes at room temperature and washed in ddH2O three times for 5 min each at room temperature. The specimen was then incubated with 1% (wt/vol) uranyl acetate (aqueous) at 4 °C for 16 hrs (overnight) and then washed in ddH_2O three times for 5 mins each time at room temperature.

Specimens were dehydrated in graded ethanol: 30, 50, 70, 90% (vol/vol) ethanol in ddH_2O for 10 mins at each step. Then samples were washed four times for 10 mins each time in 100% ethanol at room temperature. Samples were transferred to propylene oxide for 10 min at room temperature.

The specimen was finally infiltrated in a graded series of Agar100Hard in propylene oxide at room temperature: first for 1 hour in 30% (vol/vol) Agar100Hard, 1 hr in 50% (vol/vol) Agar100Hard then overnight in 75% (vol/vol) Agar100Hard, and then 100% (vol/vol) Agar100Hard for 5 hrs. After transferring samples to freshly made 100% Agar100 Hard in labelled moulds and allowed to cure at 60 °C for 72 hrs. Sections were imaged on an FEI Tecnai12 BioTwin.

NLuc activity assay

Vero cells grown in 24-well plates (Corning, 3526) were assayed for NLuc activity by adding 1 µL of coelenterazine (final concentration 1.5 µM). For 96 well formats, cell lines were seeded in white walled microwell plates (Nunc™ MicroWell™ 96-Well, Nunclon Delta-Treated, Flat-Bottom Microplate, Thermo Fisher Scientific, Paisley, UK# 136101). To measure NLuc activity, 0.5 µL coelenterazine was added per well (final concentration 3 µM). Light production was measured using filter cubes #114 and #3 on the Synergy Neo2 Multi-Mode Reader (Biotek), readings for each well were integrated over 200 ms with 4 replicate measurements per well (Gain 135 and read height 6 mm). For viability measurements, 2.5 µL Prestoblue (Thermo Fisher Scientific, Paisley UK) was added per well incubated for 10 mins before reading fluorescence at Excitation: 555/20 nm, Emission: 596/20 nm (Xenon flash, Lamp energy low, Gain 100 and read height 4.5 mm, 10 measurements per data point).

Drug screens

The DiscoveryProbe FDA-approved library of 1971 compounds (L1021, APExBIO Boston, US) was prepared as follows. After thawing the library for 4 hours at room temperature the library was arrayed into 96 well plates at 1 mM in DMSO and stored at -20 °C. Stocks (1 mM) were thawed at room temperature for 2 hrs before compounds were added to cells.

For all drug screens and validation, 5000 cells were seeded in 50 µL of growth medium for 24 hrs in white walled microwell plates. DMEM containing 2% FBS was used for Vero cells and alphaMEM containing 10% FBS was used for HUH7 cells. The following day 0.5 µL of each compound (final concentration 10 µM) was added per well and incubated for 24 hours. Eighty-eight compounds were tested per plate and each plate contained the following controls: two untreated wells, two DMSO treated wells, and one well treated with 10 µM puromycin to kill cells. SARS-CoV-2-ΔOrf7a-NLuc virus was added to all wells. In addition, two wells did not contain any cells but were infected with the SARS-CoV-2-ΔOrf7a-NLuc virus as a measure of background NLuc activity. A final well which contained cells but were uninfected were also included. Twenty-four hours after drug treatment, cells were infected with 100 PFU per well SARS-CoV-2-ΔOrf7a-NLuc virus in 50 µL of the indicated growth medium for 72 hrs. To assess virus replication and viability, 2.5 µL of Prestoblue was added to each well and plates incubated for 10 mins at 37 °C. Coelenterazine was then added to a final concentration of 3 µM. Plates were sealed prior to reading luciferase activity and viability as described above. Validation of hits were performed using the same procedures described for the drug screen.

Study design

Raw luciferase luminescence reads (x) were normalised relative to the virus-infected drug-untreated controls (u) and plate minimum read (m) on each plate by the formula:

$$x_{norm} = \frac{x_{raw} - m}{u - m}$$

This meant that a normalised luciferase value of 1 implied no difference from untreated virus replication, and a value of 0 represented total inhibition of viral replication.

The PrestoBlue reads (p) were normalised relative to the virus-infected DMSO-treated controls (d) and plate minimum read (n) on each plate by the formula:

$$p_{norm} = \frac{p_{raw} - n}{d - n}$$

This meant that a normalised PrestoBlue value of 1 implied no difference in cell viability from DMSO-treated virus infected cells, and a value of 0 representing maximal reduction in cell viability.

Compounds were categorised as either inhibitors or enhancers of NLuc-SARS-CoV-2 activity from the drug screens depending on the following criteria. Inhibitors were compounds where normalised NLuc-SARS-CoV-2 levels (x_{norm}) was reduced such that $x_{norm} < 0.15$, and cell viability as measured by normalised PrestoBlue

levels (p_{norm}) wasn't affected by more than 50%, such that $p_{norm} > 0.5$. Enhancers were compounds where normalised NLuc-SARS-CoV-2 levels (x_{norm}) was increased such that $x_{norm} > 1.5$, and cell viability as measured by normalised PrestoBlue levels (p_{norm}) wasn't affected by more than 50%, such that $p_{norm} > 0.5$.

This produced a list of 61 inhibitors and 32 enhancers in the initial VERO cells screen. Since we screened nearly 2,000 compounds, it is reasonable to question whether this initial list contained a number of false positives. However, due to the further screening and dose-response testing, we can be confident in the results presented.

Statistical analysis

Normalised luminescence values were then tested using Mathematica's *LocationTest* function, which applied either a T-test or MannWhitney test as applicable to test whether the results were significantly below 0.05 (for inhibitor hits) or significantly above 1.5 (for promotor hits). The resultant p-values were then false discovery rate (FDR) corrected using the Benjamini-Hochberg q-value procedure with an FDR of 0.1. Results with a PrestoBlue normalised value of 0.5 or below were discarded.

Role of the funding source

The funder had no role in the design of the study or the interpretation of the results. The funder did not see the manuscript prior to publication.

Results

Generation of a traceable SARS-CoV-2 virus

To monitor the replication of SARS-CoV-2 we generated DNA sequences that encode the SARS-CoV-2 variant Wuhan-Hu-1 (NC_045512.2, wild-type) and a modified traceable virus where Orf7a is replaced with the sequence encoding NanoLuciferase (SARS-Cov-2-ΔOrf7a-NLuc, **Figure 1A**). NanoLuciferase (NLuc) is an enzyme that produces light when supplied with its substrate (coelenterazine) and is readily detectable even at low quantities[2]. Orf7a has been removed in SARS-CoV and SARS-CoV-2 and yielded infectious viral clones [4-6], it is not highly conserved in beta-coronaviruses, and several disrupting mutations of Orf7a of the non-structural protein are known [7]. To generate virus particles, the DNA sequences were transcribed to RNA using T7 polymerase and electroporated into a packaging cell line, 293T cells. NLuc activity was detectable after one day and levels continued to increase up to day 5, at which point evidence of cell death was observed (**Supplemental Figure 1**). Following initial recovery of the virus, SARS-CoV-2 and SARS-CoV-2-ΔOrf7a-NLuc viruses were amplified and passaged in Vero cells. Plaque forming assays showed equivalent titres and plaque size (**Figure 1B**) and analysis of viral RNAs in the culture medium of infected cells confirmed virus production (**Supplemental Figure 1**). Virus particles were amplified and maintained by passaging in Vero cells. The activity of the reporter enzyme NLuc increased day on day allowing the replication of the virus to be monitored (**Supplemental Figure 1**). Electron microscopy demonstrated that the modified virus was structurally identical to virus recovered from wild type sequences and was detected in the same cellular compartments (**Figure 1C-D, Supplementary Figure 2**). NLuc activity was readily detected in infected cultures upon addition of the substrate coelentrazine (**Figure 1E**). With continued exposure of Vero cells to the modified virus, NLuc activity increased over several days (**Supplementary Figure 1**).

NLuc activity as a marker of virus replication

The replication of SARS-CoV-2-ΔOrf7a-NLuc was examined by exposing Vero cells to increasing numbers of replicative virus particles (PFU) and measuring bioluminescence in the presence of coelentrazine at 24, 48 and 72 hours post infection (h.p.i.). SARS-CoV-2-ΔOrf7a-NLuc virus and coelentrazine in the absence of cells were used as input controls (**Figure 2A**). The results showed a lag in virus replication of at least 48 hrs but marked replication at 72 hrs. Two hundred PFU (multiplicity of infection, MOI 0.04) induced a significant increase in NLuc activity after 48 hours; however, this only represented a small increase over the input NLuc activity that is added with the virus. Addition of as little as 2 PFU per well (MOI 0.0004), could be readily detected 72 h.p.i (**Figure 2B**), clearly demonstrating viral replication. Therefore, 72 h.p.i. was chosen as the time point at which to assess virus replication in subsequent assays. This timing of virus infection was consistent for all passages of the traceable virus, and plaque forming assays demonstrated the same replication of the wild-type and modified virus (**Figure 1, Supplementary Figure 3**). The bioluminescence signal also closely correlated with cell number (**Supplementary Figure 4**).

SARS-CoV-2 replication screen validation

High throughput screens have been developed to identify drugs suitable for re-purposing for treatment of COVID19 [8-10]. These screens have been performed in non-human cell lines, such as Vero, and rely on secondary factors such as cell viability to identify candidates, or markers that indicate virus infection. A first step in validating our viral replication screen was to measure virus replication after treatment with interferon alpha 2 (IFNA2) which has previously demonstrated to reduce virus replication [5]. When Vero cells were infected with a single PFU, pre-treatment of IFNA2 was able to reduce replication of SARS-CoV-2-ΔOrf7a-NLuc in a dose dependent manner. However, with higher virus load (100 PFU), IFNA2 had little effect on virus replication (**Figure 2C and D**). These results provided confidence that the NLuc-tagged virus system could be used to quantify the effects of drugs on virus replication, especially if reduction of bioluminescence was detected with high PFU.

Drug repurposing to target SARS-CoV-2 replication

Using a 1971 FDA-approved compound library we pretreated Vero cells before addition of 100 PFU (MOI 0.02) SARS-CoV-2-ΔOrf7a-NLuc as outlined in **Figure 3A**. Compounds that reduced virus replication by at least 85% and maintained cell viability were identified (**Figure 3B** and **Supplementary Table 3**); cell viability was determined in a duplicate screen performed with 1PFU per well (**Figure 3C**) and identified 69 compounds that reduced NLuc activity (All hits FDR<0.1 compared to untreated and DMSO controls, 55 showed no viral replication, FDR>0.1 when compared to background activity) and 29 compounds increased activity by greater the 50% (7 compounds, FDR<0.1). Five of these compounds were false positive hits due to direct inhibition of NLuc activity (**Figure 3C**, **Supplemental Table 4**).

Drug repurposing screen for SARS-CoV-2 replication in human cells

Having established an effective screening strategy in Vero cells, we sought to establish a similar approach in a human cell line capable of supporting SARS-CoV-2 replication. SARS-CoV-2 has been reported to infect multiple cell lines, and replication of the viral genome has been identified [11]. We tested the replicative capacity of SARS-CoV-2-ΔOrf7a in the lung epithelial cell lines Calu3, A549, and 16HBEo lung epithelial cells and lung fibroblasts we only observed modest virus replication as indicated by increases in bioluminescence compared to background (**Figure 4A**). We confirmed SARS-CoV-2 and SARS-CoV-2-ΔOrf7a-NLuc infection of these cell lines by real-time PCR and western blotting for the SARS-CoV-2 nucleocapsid protein (**Supplemental Figure 5**), suggesting the virus can infect but cannot replicate in these cells. To ensure a robust assay for drug screening purposes we next assessed additional cell lines reported to be infected by SARS-CoV-2, including Caco-2 [9,11] and HUH7 [12] and as we were able to recover virus particles from 293T cells we also examined replication in additional kidney cell lines, especially as the kidney is reported to express high ACE2 levels [13]. Replication in monocytic cells and fibroblastic cell lines was also monitored due to the systemic nature of COVID-19. The results showed that replication was readily observed in HUH7 cells, microvascular cells of the kidney glomerulus, and proximal tubule cells of the kidney (**Figure 4A**). The NLuc activity in infected HUH7 was up to 4-fold higher than background NLuc activity suggesting a lower rate of replication in HUH7 than in Vero cells where the signal-to-noise ratio was between 50-200 higher than background (**Supplemental Figure 3**).

We wanted to explore in more detail the apparent absence of pronounced virus replication in lung epithelial cells. As each cell line has a specific culture medium for optimal growth, we set out to test if different media could support cell growth and virus replication in lung epithelial cells. We used 15 different medium conditions to grow lung epithelial cells prior to infection with SARS-CoV-2-ΔOrf7a-NLuc. For comparison, HUH7 cells were included in the study. The results continued to show poor virus replicative capacity of lung epithelial cells. However, enhanced replication was observed in HUH7 grown in alpha-MEM, RPMI and DMEM:F12 (**Figure 4B and C**). With these optimised conditions and a signal-to-noise ratio comparable to that observed with Vero cells we screened the 1971 FDA-compound library and identified 223 compounds that suppressed SARS-CoV-2 replication by greater than 85% whilst maintaining cell viability. We refined these hits by overlapping with positive hits from the screen in Vero cells (**Figure 4E**, **Supplemental Table 5**). We identified 35 inhibitory compounds and 2 compounds that increased NLuc activity and were in common between the two screens (**Figure 4F**). The intended clinical use or targets of the 35 inhibitory compounds included anti-virals, antibiotics, modifiers of dopamine and estrogen receptor activity, calcium ion channel inhibitors and HMG-CoA reductase inhibitors (**Figure 5A**). However, also identified was a number of commonly available compounds the anti-histamine, ebastine and vitamin D3. Multiple vitamin D related compounds were present in the screen and these too suppressed SARS-CoV-2-ΔOrf7a-NLuc although these did not all meet our criteria for both Vero and human cell lines. In addition to inhibitory compounds, we identified two compounds that increased NLuc activity, this could represent enhanced uptake of the virus or enhanced viral replication, these included aliskerin and litholicholic acid, on further inspection of the inducers of the virus signal we also observed

In our studies, inhibitors were identified by treatment of cells *prior* to infection. To identify whether any of these hits could also *prevent* replication in cells already infected with SARS-CoV-2-ΔOrf7a-NLuc, we infected

Vero cells with SARS-CoV-2 for 24 hrs (sufficient time for the virus to begin replication) then added each of the 35 inhibitor compounds. The cells were incubated for 48 hrs (i.e. a total of 72 h.p.i) and bioluminescence was measured. The majority of the compounds had no impact on virus replication; after excluding NLuc inhibitors, we identified 9 of the 35 compounds reduced replication relative to DMSO (Table 1, **Supplemental Figure 6**). The effective doses for these compounds were then determined in HUH7 cells (**Figure 5**, **Table 1**), and whilst these are preliminary data these demonstrate that these compounds have efficacy in reducing virus replication after infection and warrant further investigation to determine if these could ease the burden of the virus in patients.

Table 1: Approved uses of the 9 compounds of interest that inhibit SARS-CoV-2 infection and replication in HUH7 cells.

Compound	HUH7 IC50	Vero IC50	Post-infection at IC50	Approved Use	Target
Panobinostat	<0.2 µM	<0.2 µM	-25%	Multiple myeloma	HDAC inhibitor
LY2835219	0.2 µM	1 µM	-40%	Abemaciclib for advanced breast cancer	CDK4/6 inhibitor
Manidipine	2 µM	7.5 µM	-50%	Anti-hypertensive	Calcium channel blocker
Manidipine 2HCl	2.5 µM	7.5 µM	-50%	Anti-hypertensive	Calcium channel blocker
Ebastine	0.5 µM	5 µM	-25%	Anti-histamine for allergic rhinitis and chronic idiopathic urticaria	H_1 receptor blocker
Atovaquone	7.5 µM	3 µM	-25%	antimicrobial (anti-malarial)	mitochondrial electron transport
Bedaquiline	5 µM	10 µM	-30%	pulmonary tuberculosis	mycobacterial ATP synthase
Vitamin D3	3 µM	10 µM	-30%	Common supplement	Transcriptional/calcium regulation
Amodiaquine	1 µM	5 µM	-25%	antimicrobial (anti-malarial)	Inhibitor heme polymerase activity

Discussion

In this study we have shown, 1) that the SARS-CoV-2 virus infects and replicates in a range of human cells but especially hepatocytes, kidney glomerulus, and proximal tubule cells of the kidney, 2) that 9 drugs that have previously been shown to be safe in humans and approved by the FDA for clinical use are effective in inhibiting SARS-CoV-2 infection and replication even when used post-infection, and 3) 2 drugs in common use enhance

SARS-CoV-2 infection and replication in human hepatocytes. Whilst our study has focused on SARS-CoV-2 infection and replication in cells in culture, the alignment of liver and kidney cells as particular targets of SARS-CoV-2 infection with observations of liver and kidney damage in patients with COVID-19, suggest that the COI identified here warrant investigation in patients.

Liver comorbidities has been reported in 2-11% of patients with COVID-19 and 14-53% of cases reported abnormal levels of liver enzymes [14], with liver injury being more prevalent in severe cases (reviewed by [15]). Another study reported that patients with chronic liver disease, especially African Americans, were at increased risk of COVID-19 [16]. It has been suggested that liver damage in patients with COVID-19 might be caused by viral infection of liver cells, which is supported by the presence of SARS-CoV-2 RNA in stool [17]. Whilst establishing if liver damage is the direct result of COVID infection is sometimes difficult, evidence that SARS-CoV-2 can replicate in liver cells might help in the management of COVID patients with pre-existing liver disease. On a related note, there is discrepancy in the literature about whether SARS-CoV-2 can replicate in, and can be recovered from, HUH7 cells (e.g. [12,18]). Discrepancies might arise because of the use of different cell culture conditions or sensitivity of detection. However, our data showing that HUH7 cells are as competent as Vero cells (which are a popular cell of choice for studying virus infection) in supporting SARS-CoV-2 infection and replication leading to cytopathic effects, point to a direct mechanism to explain liver abnormalities in patients with COVID-19. On a similar note, acute kidney injury is a common complication of COVID-19, and has been associated with increased morbidity and mortality (reviewed by [19]). Our data showing SARS-CoV-2 infection and replication in kidney cells indicates a molecular mechanism for kidney pathology and cell death.

Turning to our COI, some have known mechanisms of actions and intracellular protein targets that might be expected to be utilised by SARS-CoV-2 in its infection and replication life cycle. Among these is Panobinostat, which is a HDAC inhibitor that blocks DNA replication, which are a class of compounds used to inhibit cell growth in the management of cancer. Panobinostat had the strongest effect on limiting SARS-CoV-2 replication whilst maintaining cell viability, and completely blocked replication of SARS-CoV-2 at all doses tested (**Figure 5**); however, if cells were infected prior to treatment a more modest effect on replication were observed. This difference may be related to the recent observations that suggest that Panobinostat can suppress ACE2 expression [20], which would explain its beneficial effect prior to entry of the virus into cells and not thereafter. abemaciclib (LY2835219) is another cell cycle inhibitor, suppressor of DNA replication and anti-cancer drug that emerged from the screen. Atovaquone is a competitive inhibitor of the mitochondrial electron transport chain and is approved for use in treating chest infections such as pneumocystis pneumonia and malaria. Inhibition of energy production in the cell might be expected to impact on the virus' ability to highjack cellular machinery for its replication. Our observation that bedaquiline inhibits SARS-CoV-2 replication supports evidence from an in silico repurposing study in which bedaquiline was proposed to be a promising inhibitor of the main viral protease of SARS-CoV-2 [21]. Furthermore, inhibitors to the main protease have proved effective in inhibiting replication of SARS-CoV-2 in Vero 76 cells [22].

COI with functions other than arrest of cell cycle or blockade of metabolism include manidipine (a calcium ion channel blocker approved for the use in treating hypertension), ebastine (a second generation H1 receptor antagonist that has been approved for the treatment of allergic rhinitis and chronic idiopathic urticaria), and vitamin D3, which is a health supplement that is available over the counter. The reasons why these compounds are effective in reducing SARS-CoV-2 infection and replication are unclear, but their low toxicity, absence of cytopathic effects, and widespread availability (especially for vitamin D3) warrants closer investigation as a prophylactic measure in the prevention of COVID. For example, the vitamin D receptor (VDR, a member of the nuclear hormone receptor superfamily) is proposed to be essential for liver lipid metabolism because its deficiency in mice protects against hepatosteatosis [23]. Once bound to VDR, vitamin D plays a major role in hepatic pathophysiology, regulation of innate and adaptive immune responses, and might contribute to anti-proliferative, anti-inflammatory and anti-fibrotic activates (reviewed by [24]). Thus far, whether vitamin D supplementation reduces the risk of infection or disease severity is unclear [25], and may relate to the multiple

forms of vitamin D. Whilst vitamin D3 met the stringent cut-offs of 85% virus reduction, vitamin D2 also reduced virus replication.

Of the two drugs that we found to enhance SARS-CoV-2 infection and replication, aliskiren is particularly noteworthy. Aliskiren is a potent inhibitor of renin, which is part of the Renin-Angiotensin-Aldosterone System (RAAS) for the regulation of blood pressure, fluid balance and systemic vascular resistance. Under normal circumstances, renin converts angiotensinogen to angiotensin 1 (1-10), which is a substrate for ACE1 and ACE2. ACE1 generates angiotensin II (Ang 1-8), which binds to the AT1 and AT2 receptors to mediate vasoconstriction and elevation of blood pressure via a calcium ion mediated mechanism. In fact, increased AngII levels have been observed in the lungs of SARS-challenged mice [26]. ACE2 cleaves AngI to generate peptides that bind the Mas receptor (which forms a heterodimer with the bradykinin BK2 receptor [27]), resulting in increased vascular leakage and angioedema. Although ACE2 is a primary receptor for SARS-CoV-2, studies in mouse models of acute respiratory distress syndrome have shown that absence of ACE2 results in a more severe phenotype, while over expression of ACE2 had some protective effect [28]. Taken together, inhibition of renin in the presence of SARS-CoV-2 could disrupt the balance of the RAAS system resulting in elevated levels of cellular infection by SARS-CoV-2.

In conclusion, our study has identified 9 compounds that are safe in humans and show effectiveness in reducing SARS-CoV-2 infection and replication in human cells, especially hepatocytes. Their potency in stopping the virus replicating in human cells, especially as the COVID pandemic continues on a worldwide scale, warrants a study of the efficacy of these COI in humans.

Contributors

AP co-conceived the project, performed the experiments, interpretated the data, drafted the manuscript. BCC performed experiments and interpreted the data. JC performed experiments. RG performed experiments. YL performed experiments. KEK co-conceived the project, raised the funding, drafted the manuscript. All authors approved the final manuscript.

Declaration of interests

The authors have no conflicts of interest.

Acknowledgements

The authors thank Dr. Jennifer Cavet for providing assistance with working at containing level 3 and use of the facilities. The project was approved by the COVID-19 Rapid Response Group, the R3G Research Operations Group and the R3G Executive Committee at the University of Manchester. We would also like to thank staff and students at the University of Manchester for the provision of cell lines for this study: Dr Stuart Cain, Dr Jonathan Humphries, Dr Shiu-wan Chan, Dr Chris Smith, Mrs Rachel Compton, Dr Rogerio Almeida, Dr Sara Gago, Dr Andrew Higham, and Dr Jeremy Herrera. Also thanks to Mrs Nikki-Maria Koudis, Mrs Maryline Fresquet and Dr Bernard Davenport from Professor Rachel Lennon's laboratory for help sourcing kidney cell lines. We would also like to thank Thermo Fisher Scientific for their help in providing microwell plates for this study, with special thanks to Charlotte Connor and Claire Marshall. Finally, we would like to thank Miss Anna Pickard for her illustration of the coronavirus.

Figure legends

Figure 1: Nanoluciferase (NLuc) modified SARS-CoV-2 virus as a reporter for virus replication.

A) Diagram of the SARS-CoV-2 genome, highlighting the insert site for the reporter NLuc in place of Orf7a, (SARS-CoV-2-ΔOrf7a-Nluc).

B) Virus particles recovered following transfection of wild-type (WT) or NLuc modified SARS-CoV-2 encoding RNA into 293T cells were used to infect Vero cells. The recovered virus (P1 virus) was then titred in Vero cells to assess virus replication and plaque forming potential.

C) Electron microscopy of the SARS-Cov-2 virus 72 h.p.i. of Vero cells (Passage 4, P4), both intra- and extra-cellular virus particles were identified.

D) Measurement of diameter for the wild-type (WT) and NLuc modified SARS-CoV-2 particles.

Figure 2: Timings of SARS-CoV-2-ΔOrf7a-NLuc virus replication.

A) Schematic showing how SARS-CoV-2 ΔOrf7a-NLuc was used to assess virus replicaiton. During virus replication as virus particles are released from the cell, or as a result of cell death, NLuc activity is detected in the conditioned medium together with virus particles. In subsequent assays the NLuc activity is recorded in the absence of cells, and NLuc signals above this background noise are used to indicate the level of virus replication.

B) The replication of SARS-CoV-2-ΔOrf7a-Nluc was monitored in a miniaturised 96 well assay. Using 5000 Vero cells per well, increasing numbers of virus particles were added and monitored 24, 48 and 72 hours post infection (h.p.i). Substantial and significant increases in NLuc activity were observed when only two plaque forming units (PFU) were added, higher NLuc activity was associated with higher viral input. Even with higher viral inputs the substantial increases in NLuc activity occurred only after 72 hours infection.

C) 5000 Vero cells were pre-treated with increasing doses of IFNα2 for 24 hours prior to infection with 1PFU SARS-CoV-2-ΔOrf7a-Nluc. NLuc activity and viability were assessed 72 h.p.i. demonstrating effective inhibition of virus replication. The blue line indicates the luminescence counts per second for DMSO treated controls. N=3 replicate samples

D) As in C, 5000 Vero cells were treated with increasing doses of IFNα2 for 24 hours prior to infection with 100PFU SARS-CoV-2- ΔOrf7a-Nluc. With this higher titre virus replication was not inhibited. . The blue line indicates the luminescence counts per second for DMSO treated controls. N=3 replicate samples.

Figure 3: Screen of 1971 FDA-approved compounds to identify therapeutics that inhibit SARS-CoV-2-ΔOrf7a-NLuc virus replication.

A) Schematic of the screening procedure used to assess whether FDA-approved compounds alter SARS-CoV-2 ΔOrf7a-Nluc virus replication.

B) Performance of control samples across the 23 microwell plate screen. Each point represents the controls included on each of the microwell plates. See Methods section for description of data processing.

C) Scatterplot showing the effects of 1971 compounds on Sars-CoV-2 ΔOrf7a-NLuc replication and cell viability. Shaded boxes highlight the top 50 compounds that reduced NLuc activity and top 29 compounds that increased NLuc activity.

D) Scatterplot of the 50 compounds that reduced NLuc activity in C, and their effect in a replicate screen using 1 PFU SARS-CoV-2 ΔOrf7a-NLuc virus per well. Highlighted in green are compounds which inhibit the NLuc enzyme directly. The blue dashed line indicates the luminescence counts per second for untreated controls.

Figure 4: Replication of SARS-CoV-2-ΔOrf7a-Nluc in human cell lines.

A) SARS-CoV-2 replication in human cell lines. Five thousand cells per well were seeded and infected as in figure 3A. All cells were grown in the recommended growth medium, detailed in Table 1. The NLuc activity after 3 days was used to assess the degree of virus replication. The activity of NLuc activity above the baseline activity are shown as a heat map. Each bar is the average of 2 biological repeats of each cell line at each virus dose, with the same findings observed when 2000, or 10,000 cells were seeded.

B) Lung epithelial, fibroblasts, HUH7 and 293T cell lines were grown in 15 different growth medium compositions. NLuc activity over background three days after infection is shown. The degree of Sars-CoV-2 replication observed in HUH7 cells was similar to those observed in Vero. Each box represents 4 replicate measures of replication. Similar findings were observed in n=6 biological repeats. Each row represents a different growth medium as indicated in C).

C) NLuc activity above background three days after infection in HUH7 cells. Each box represents 4 replicate measures of replication. Similar findings were observed in n=6 biological repeats.

D) Screen of 1971 FDA-approved compound library in the human cell line HUH7 grown in alpha-MEM supplemented with 10% FBS. 5000 cells were treated with 10 µM of each compound for 24 hours prior to infection with 100 PFU of SARS-CoV-2-ΔOrf7a-NLuc (MOI 0.02). Virus replication progressed for 72 hours as in Figure 3A. NLuc activity (signal above background) was used as a measure of virus replication and cell viability at the end of the assay.

E) Comparison and overlap of inhibitors identified in the compound screening for HUH7 and Vero cells.

F) Comparison and overlap of activators identified in the compound screening for HUH7 and Vero cells.

Figure 5: Dose response of SARS-CoV-2 inhibitors.

A) Summary of the inhibitor class of the 35 compounds identified in both the Vero and HUH7 screens.

B) Effects of Vitamin D related compounds from the APExBIO DiscoveryProbe library on NLuc activity in the Vero and HUH7 screens.

C) Effects of compounds that increased NLuc activity in both Vero and HUH7 screens. Cetirizine and Cetirizine dihydrochloride also induced bioluminescence over control independently in Vero and HUH7 screens.

D) Dose responses to the 9 compounds in HUH7 cells. Cells were treated and infected as described in Figure 4D. NLuc activity relative to DMSO controls are shown in blue, and viability relative to DMSO are shown in black. N=2 independent repeats are shown.

Supplementary Figure 1: Recovery of replication competent SARS-CoV-2 from synthetic DNA constructs.

A) Schematic for the recovery of SARS-CoV-2 virus particles from DNA encoding the wild type and NLuc modified SARS-CoV-2 genome. RNA was transcribed from the synthetic DNA constructs and electroporated into 293T cells, the cells were monitored daily for NLuc activity and evidence of the cytopathic effects of virus replication. 6 days post electroporation virus containing medium was collected.

B) NLuc activity in 293T cells electroporated with wild type and NLuc modified SARS-CoV-2 RNA transcripts.

C) Real-time PCR primer validation using SARS-CoV-2 encoding DNA. NLuc coding sequences were inserted in place of the Orf7a gene. Primers designed to amplify sequences within the DNA constructs confirmed primer specificity. The number of cycles for each gene were normalised to those of the WT virus, or for NLuc to ΔOrf7a NLuc. For each DNA construct the qPCR data was also normalised to the number of cycles obtained for the N gene N=3 technical repeats.

D) Real-time qPCR detection of Viral RNAs in the medium of infected Vero cells 72 hours post infection. Vero cells were infected with Sars-CoV-2 WT (MOI 0.1) or Sars-CoV-2 ΔOrf7a-Nluc (MOI 1).

E) Initial assessment of viral replication in Vero cells. 24h post-infection NLuc activity was readily detected in SARS-CoV-2 ΔOrf7a-Nluc infected samples, N=3 replicate samples.

F) NLuc activity in Vero cells infected with wild type SARS-CoV-2 or SARS-CoV-2 ΔOrf7a-Nluc modified virus. NLuc activity was significantly elevated in SARS-CoV-2 ΔOrf7a-Nluc infected cultures across all time points, *** represents $p<0.001$ in a Students T-Test, N=3 replicate samples. With prolonged culture NLuc activity within infected samples increased approximately 30-fold.

Supplementary Figure 2: Detection of SARS-CoV-2 virus particles in Vero cells infected with passage 4 virus stocks.

A) After 4 passages of recovered wild type SARS-CoV-2 virus particles in Vero cells, naïve Vero cells were infected and fixed 72 hours post infection. Viral particles could be observed inside and outside of Vero cells indicated by red arrows. Scale bar, 2 µm.

B) Higher magnification image of an independent region of the sample in A. Scale bar, 0.5 µm.

C) After 4 passages of recovered SARS-CoV-2-ΔOrf7a-NLuc virus particles in Vero cells, naïve Vero cells were infected and fixed 72 hours post infection. Viral particles could be observed inside and outside of Vero cells indicated by blue arrows. Scale bar, 2 µm.

D) Higher magnification image of an independent region of the sample in C. Scale bar, 0.5 µm.

Supplementary Figure 3: Replication assays for different passages of SARS-CoV-2-ΔOrf7a-NLuc virus.

A) The plots show 5000 Vero cells infected with different volumes of virus harvested from repeat passages of the virus (P) in Vero cells. With increasing viral load, there is an increase in background as more NLuc activity is added to each well (Blue). The background signal arises when NLuc, expressed as the virus replicates, is released from infected cells that have lysed upon liberation of the virus particles. N=2 independent experiments.

B) After subtracting the background noise observed in wells without cells (blue in A), the additional NLuc activity generated through viral replication showed comparable signals for each virus passage. N=2 independent experiments.

C) The signal to noise ratio for each batch was used to identify the optimal conditions for virus replication for subsequent screening experiments.

Supplementary Figure 4: SARS-CoV-2-ΔOrf7a-Nluc replication optimisation

NLuc activity at different times after infection with increasing numbers of SARS-CoV-2 virus particles. Enhanced NLuc signals were observed 72 hours post infection (h.p.i) when either A) 2000, B) 5000 or C) 10,000 cells per well were used. Maximal signals were generated with 5000 cells per well, as seeding 10,000 cells tended to reduce NLuc activity. Five thousand cells were used for all subsequent assays.

Supplemental Figure 5: Detection of SARS-CoV-2 infection in lung epithelial cells.

A) Real-time PCR detection of SARS-CoV-2 nucleocapsid (N) RNA in cells 72 h.p.i. Viral RNAs were readily detected in cells infected with WT or ΔOrf7a-Nluc virus particles.

B) Western blot detection of SARS-CoV-2 nucleocapsid (N) protein in cells 72 hours post infection. Lower levels of the N protein are detected in fibroblasts and lung epithelial cells when compared to 293T and Vero cells suggesting the virus can infect but not replicate in these cell lines.

C) Real-time detection of known mediators of SARS-CoV-2 entry into cells. ACE2, NLP1 and TMPRSS2 RNA levels are shown relative to RPLP0. Infectious virus in lung cell lines but no replication.

Supplemental Figure 6: Effective compounds that suppress SARS-CoV-2 replication with treatment commencing after infection.

A) Schematic for assessing whether any compounds that suppressed virus replication prior to infection could also affect replication post-infection.

B) Fifty compounds identified to suppress SARS-CoV-2 replication in Figure 3 were assessed to identify dose-dependent effects on SARS-CoV-2 replication with treatment progressing after infection (as outlined in A). Nine compounds were found to suppress replication in a dose dependent manner.

References

1. Li W, Moore MJ, Vasilieva N, et al. Angiotensin-converting enzyme 2 is a functional receptor for the SARS coronavirus. *Nature* 2003; **426**(6965): 450-4.

2. Calverley BC, Kadler KE, Pickard A. Dynamic High-Sensitivity Quantitation of Procollagen-I by Endogenous CRISPR-Cas9 NanoLuciferase Tagging. *Cells* 2020; **9**(9).

3. Pickard A, Chang J, Alachkar N, et al. Preservation of circadian rhythms by the protein folding chaperone, BiP. *FASEB J* 2019; **33**(6): 7479-89.

4. Thi Nhu Thao T, Labroussaa F, Ebert N, et al. Rapid reconstruction of SARS-CoV-2 using a synthetic genomics platform. *Nature* 2020; **582**(7813): 561-5.

5. Xie X, Muruato A, Lokugamage KG, et al. An Infectious cDNA Clone of SARS-CoV-2. *Cell Host Microbe* 2020; **27**(5): 841-8 e3.

6. Xie X, Muruato AE, Zhang X, et al. A nanoluciferase SARS-CoV-2 for rapid neutralization testing and screening of anti-infective drugs for COVID-19. *Nat Commun* 2020; **11**(1): 5214.

7. Rosenthal SH, Kagan RM, Gerasimova A, et al. Identification of eight SARS-CoV-2 ORF7a deletion variants in 2,726 clinical specimens. *bioRxiv* 2020.

8. Riva L, Yuan S, Yin X, et al. Discovery of SARS-CoV-2 antiviral drugs through large-scale compound repurposing. *Nature* 2020; **586**(7827): 113-9.

9. Touret F, Gilles M, Barral K, et al. In vitro screening of a FDA approved chemical library reveals potential inhibitors of SARS-CoV-2 replication. *Sci Rep* 2020; **10**(1): 13093.

10. Jeon S, Ko M, Lee J, et al. Identification of Antiviral Drug Candidates against SARS-CoV-2 from FDA-Approved Drugs. *Antimicrob Agents Chemother* 2020; **64**(7).

11. Chu H, Chan JF, Yuen TT, et al. Comparative tropism, replication kinetics, and cell damage profiling of SARS-CoV-2 and SARS-CoV with implications for clinical manifestations, transmissibility, and laboratory studies of COVID-19: an observational study. *Lancet Microbe* 2020; **1**(1): e14-e23.

12. Zhou P, Yang XL, Wang XG, et al. A pneumonia outbreak associated with a new coronavirus of probable bat origin. *Nature* 2020; **579**(7798): 270-3.

13. Wysocki J, Lores E, Ye M, Soler MJ, Batlle D. Kidney and Lung ACE2 Expression after an ACE Inhibitor or an Ang II Receptor Blocker: Implications for COVID-19. *J Am Soc Nephrol* 2020; **31**(9): 1941-3.

14. Huang C, Wang Y, Li X, et al. Clinical features of patients infected with 2019 novel coronavirus in Wuhan, China. *Lancet* 2020; **395**(10223): 497-506.

15. Zhang C, Shi L, Wang FS. Liver injury in COVID-19: management and challenges. *Lancet Gastroenterol Hepatol* 2020; **5**(5): 428-30.

16. Wang Q, Davis P, Xu R. COVID-19 risk, disparities and outcomes in patients with chronic liverdisease in the United States. *EClinicalMedicine* 2020.

17. Yeo C, Kaushal S, Yeo D. Enteric involvement of coronaviruses: is faecal-oral transmission of SARS-CoV-2 possible? *Lancet Gastroenterol Hepatol* 2020; **5**(4): 335-7.

18. Ogando NS, Dalebout TJ, Zevenhoven-Dobbe JC, et al. SARS-coronavirus-2 replication in Vero E6 cells: replication kinetics, rapid adaptation and cytopathology. *J Gen Virol* 2020; **101**(9): 925-40.

19. Braun F, Lutgehetmann M, Pfefferle S, et al. SARS-CoV-2 renal tropism associates with acute kidney injury. *Lancet* 2020; **396**(10251): 597-8.

20. He B, Garmire L. Prediction of repurposed drugs for treating lung injury in COVID-19. *F1000Res* 2020; **9**: 609.

21. Ferraz WR, Gomes RA, AL SN, Goulart Trossini GH. Ligand and structure-based virtual screening applied to the SARS-CoV-2 main protease: an in silico repurposing study. *Future Med Chem* 2020; **12**(20): 1815-28.

22. Ma C, Sacco MD, Hurst B, et al. Boceprevir, GC-376, and calpain inhibitors II, XII inhibit SARS-CoV-2 viral replication by targeting the viral main protease. *Cell Res* 2020; **30**(8): 678-92.

23. Bozic M, Guzman C, Benet M, et al. Hepatocyte vitamin D receptor regulates lipid metabolism and mediates experimental diet-induced steatosis. *J Hepatol* 2016; **65**(4): 748-57.

24. Triantos C, Aggeletopoulou I, Thomopoulos K, Mouzaki A. Vitamin D - liver disease association: Biological basis and mechanisms of action. *Hepatology* 2021.

25. The Lancet Diabetes E. Vitamin D and COVID-19: why the controversy? *Lancet Diabetes Endocrinol* 2021; **9**(2): 53.

26. Raudies O, Kuban RJ, Hamacher F, et al. Functional analysis and secondary expression profiling of candidate genes deregulated in conjunction with oncogenic Ras signaling. *Adv Enzyme Regul* 2005; **45**: 63-84.

27. Cerrato BD, Carretero OA, Janic B, Grecco HE, Gironacci MM. Heteromerization Between the Bradykinin B2 Receptor and the Angiotensin-(1-7) Mas Receptor: Functional Consequences. *Hypertension* 2016; **68**(4): 1039-48.

28. Imai Y, Kuba K, Rao S, et al. Angiotensin-converting enzyme 2 protects from severe acute lung failure. *Nature* 2005; **436**(7047): 112-6.

Figure 1 (Pickard et al.)

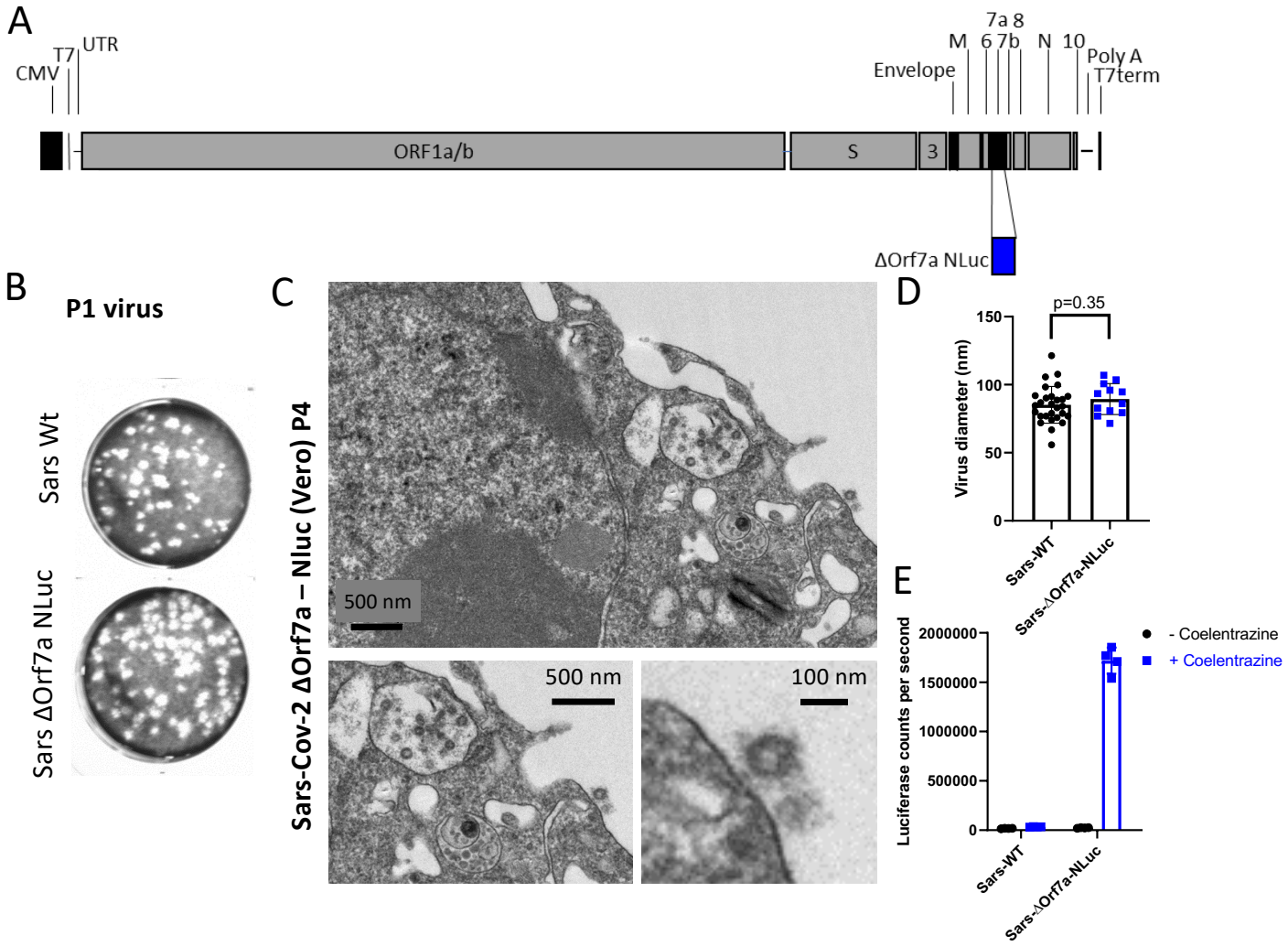

Figure 2 (Pickard et al.)

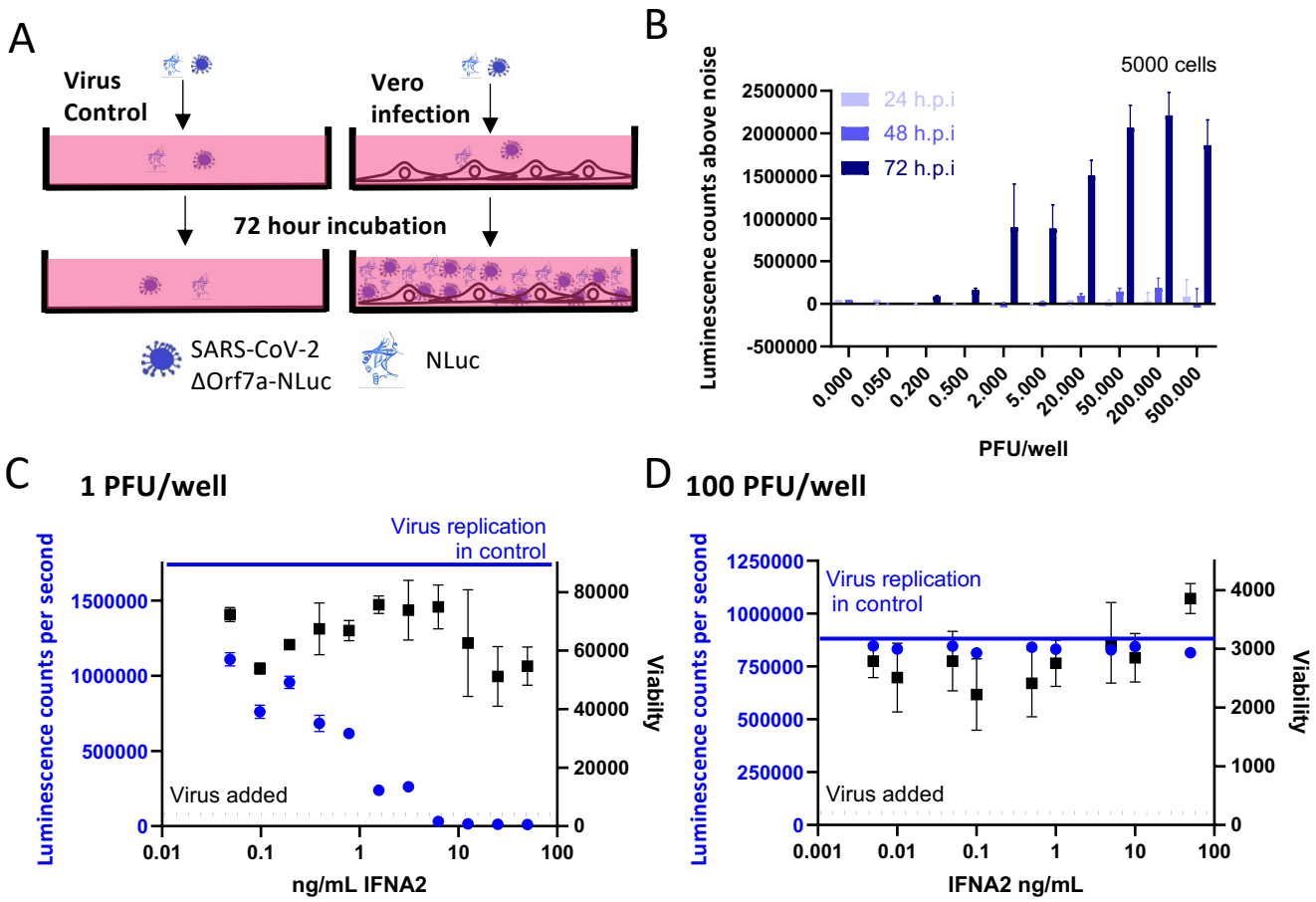

Figure 3 (Pickard et al.)

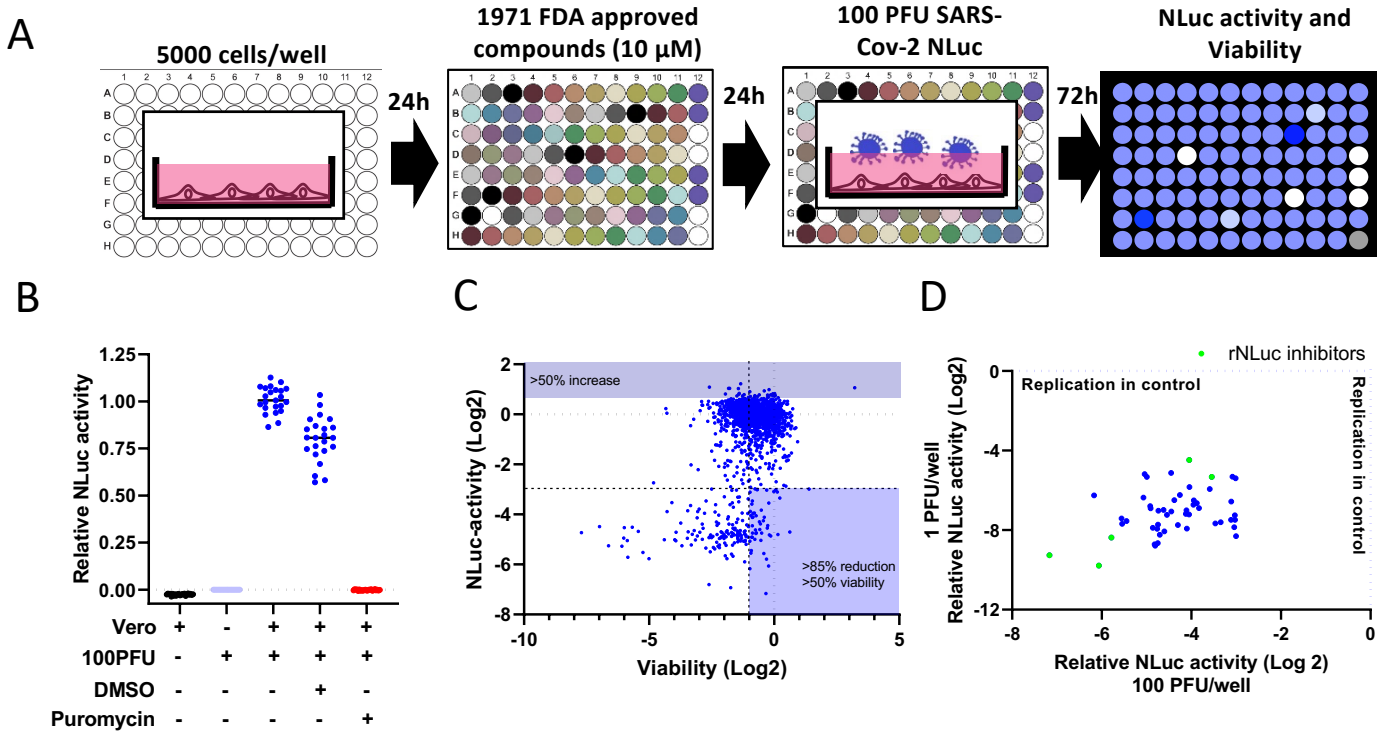

Figure 4 (Pickard et al.)

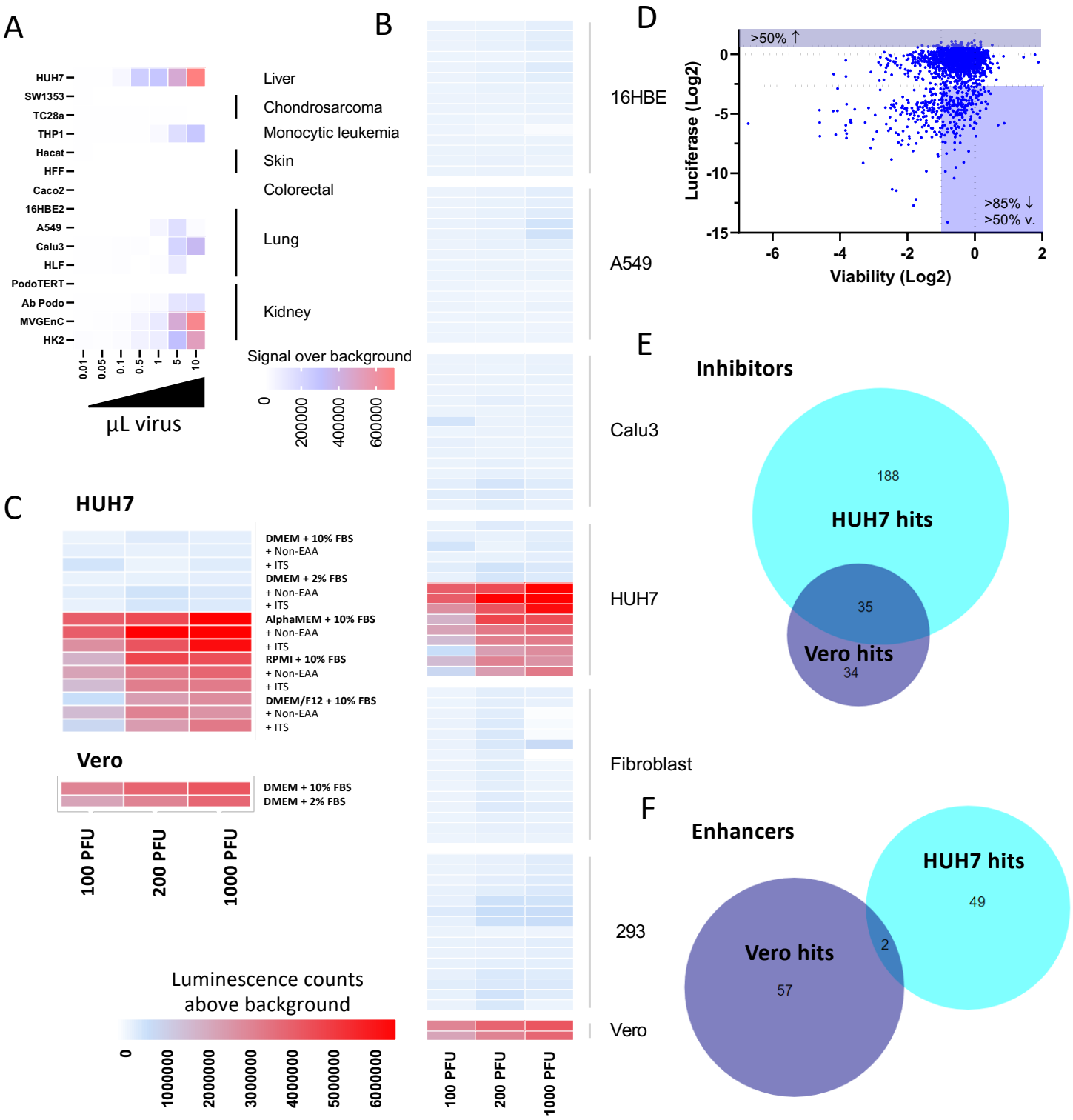

Figure 5 (Pickard et al.)

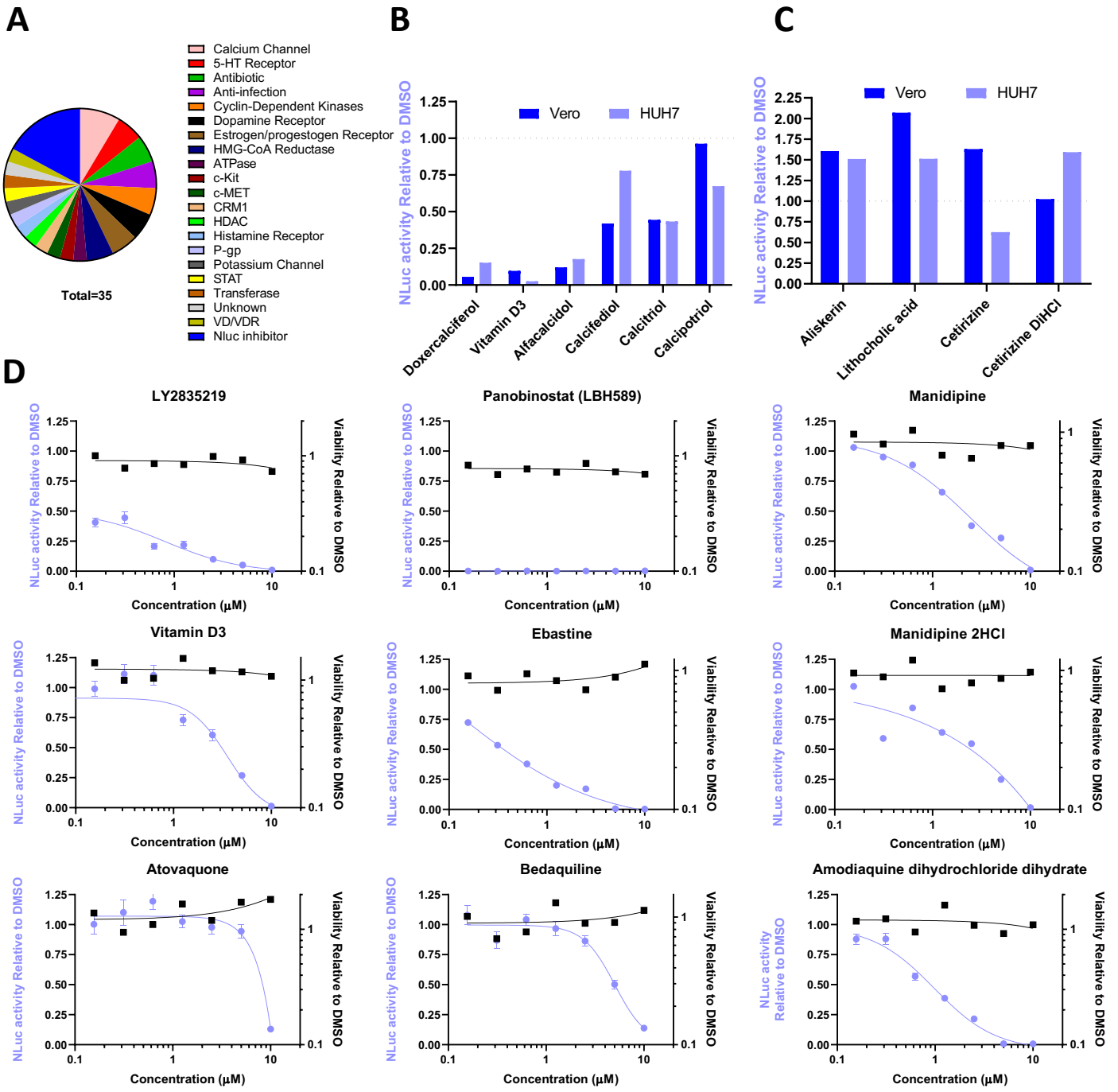

Supplemental Figure 1 (Pickard et al.)

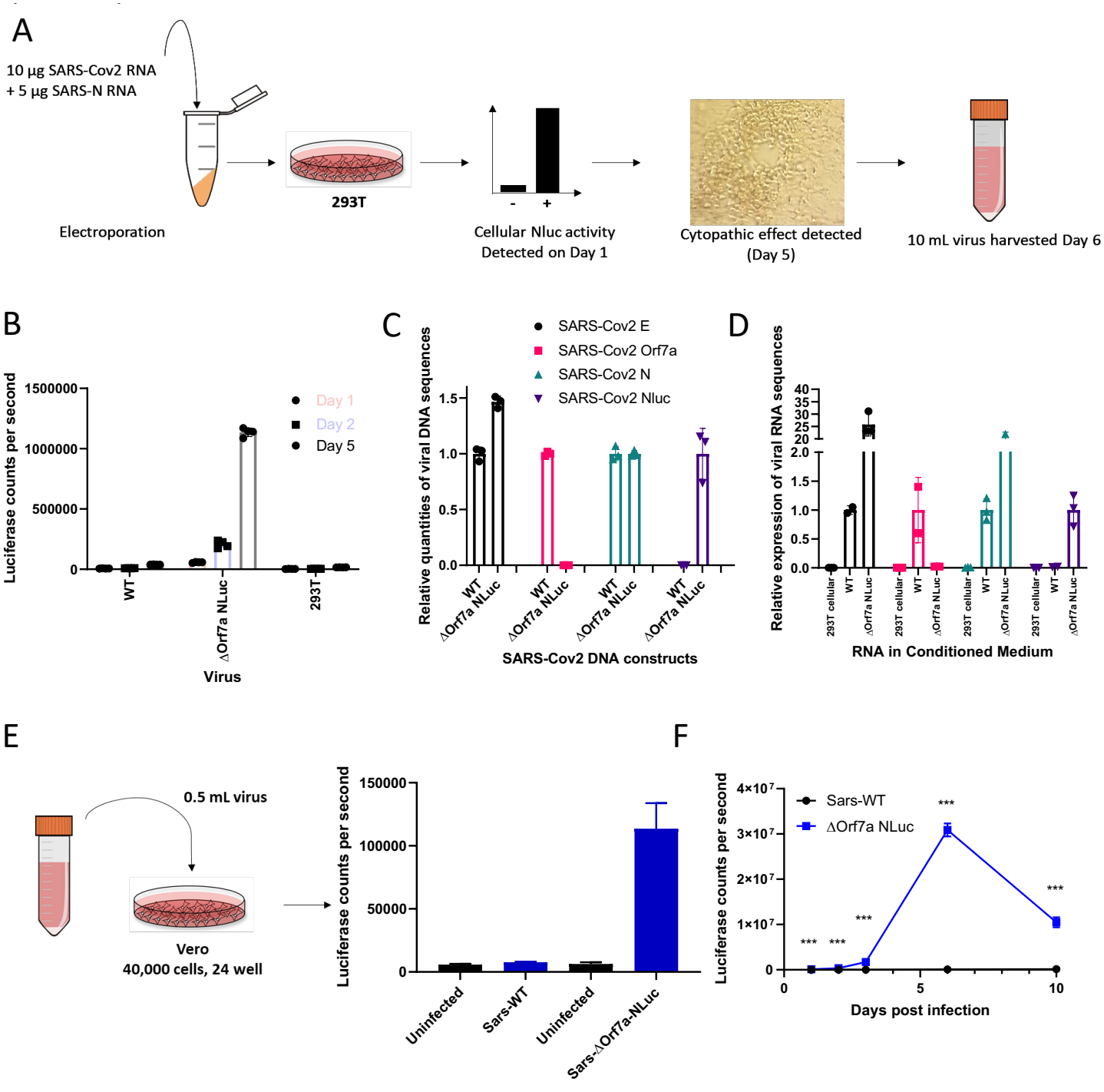

Supplemental Figure 2 (Pickard et al.)

A) SARS-CoV-2 (wild type)

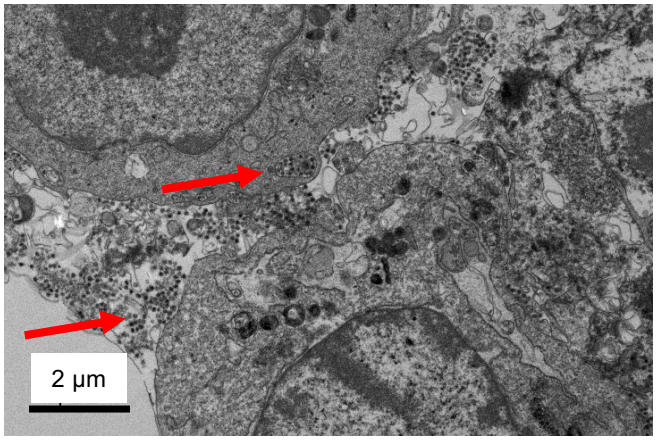

B) SARS-CoV-2 (wild type)

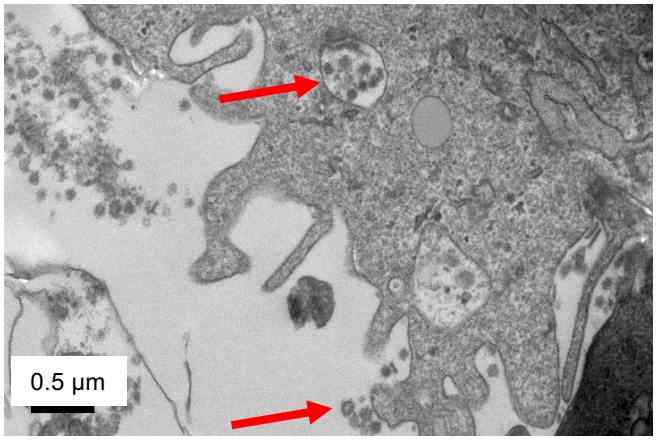

C) SARS-Cov-2-ΔOrf7a–NLuc

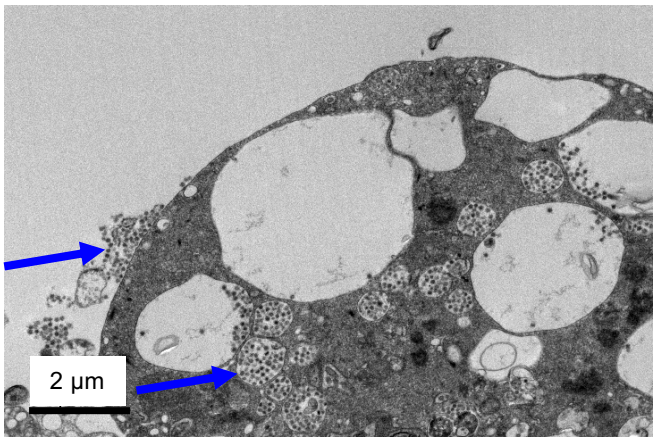

D) SARS-Cov-2-ΔOrf7a–NLuc

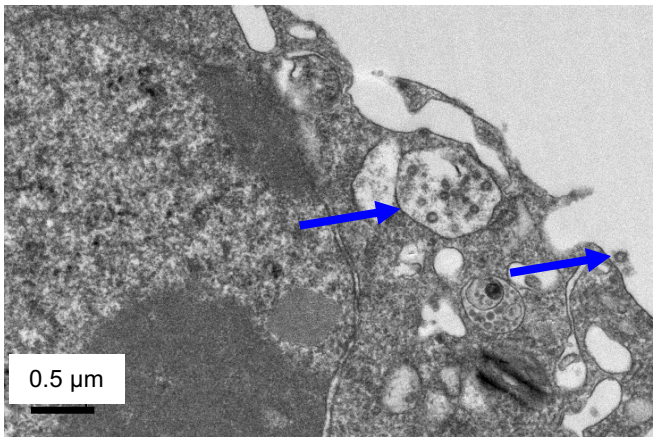

Supplemental Figure 3 (Pickard et al.)

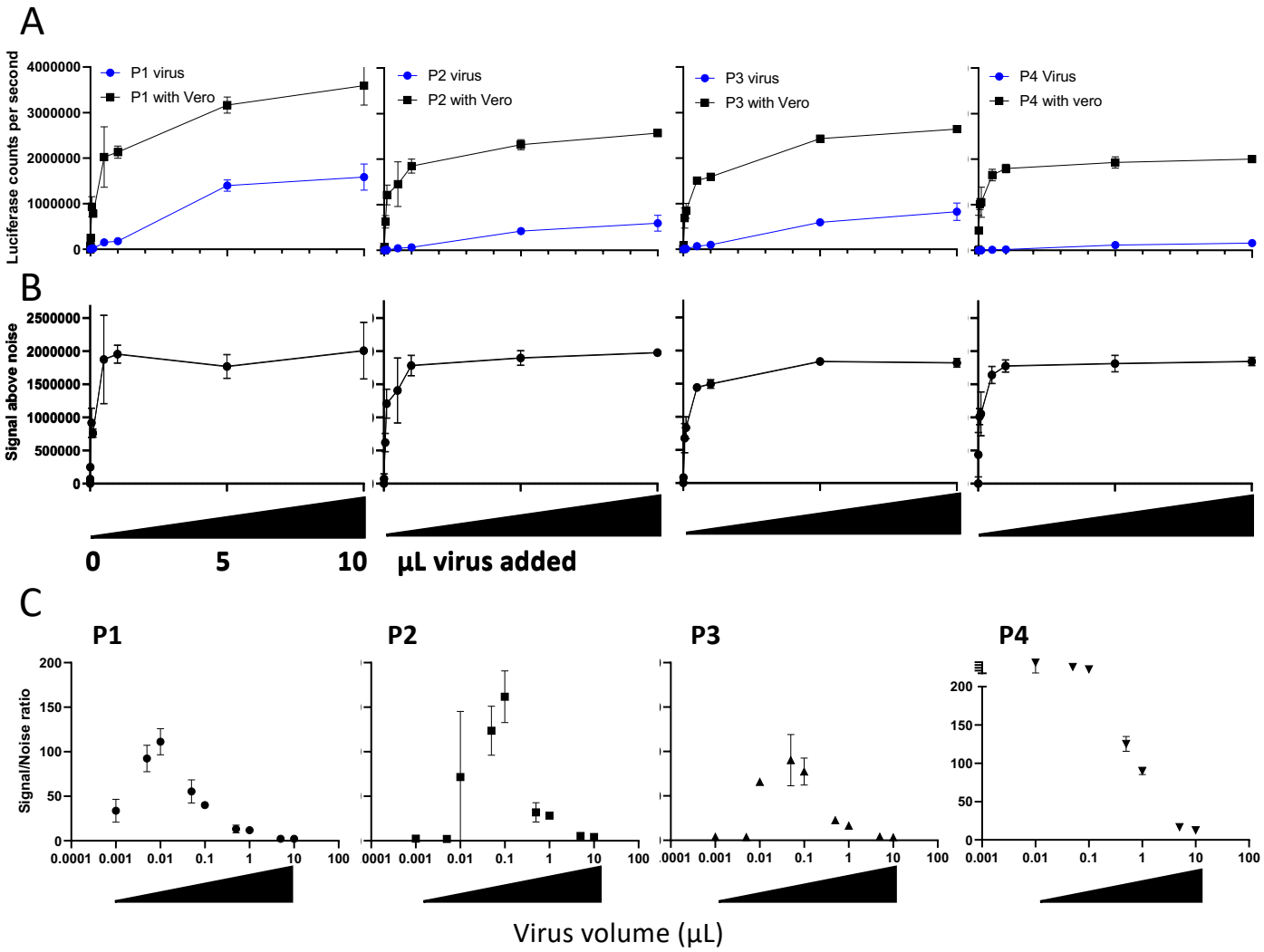

Supplemental Figure 4 (Pickard et al.)

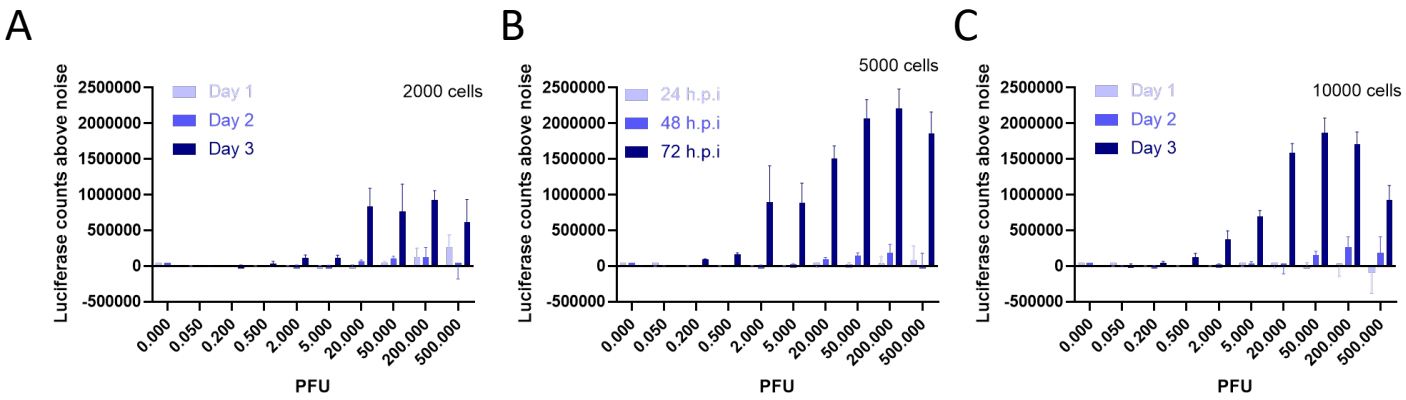

Supplemental Figure 5 (Pickard et al.)

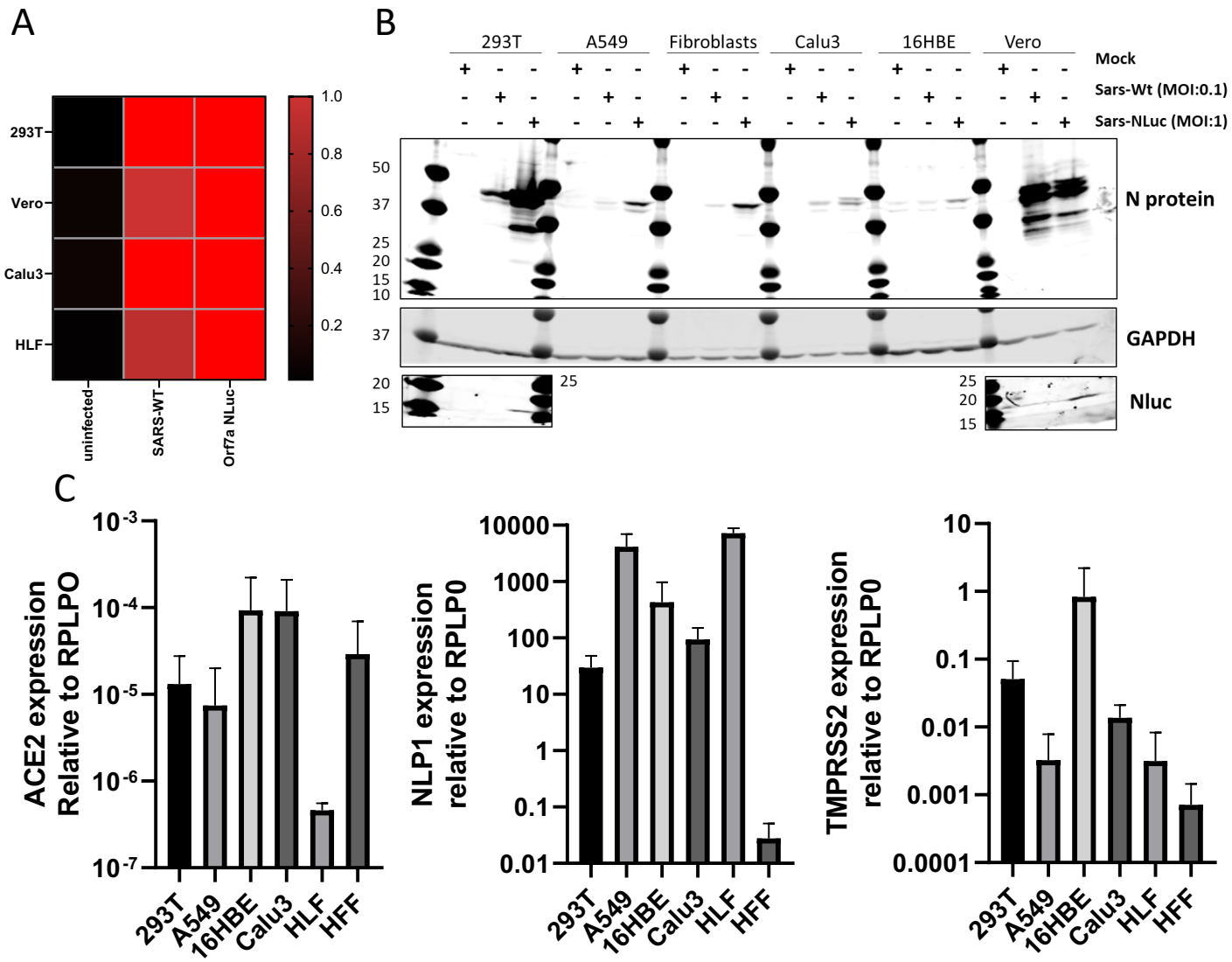

Supplemental Figure 6 (Pickard et al.)

A

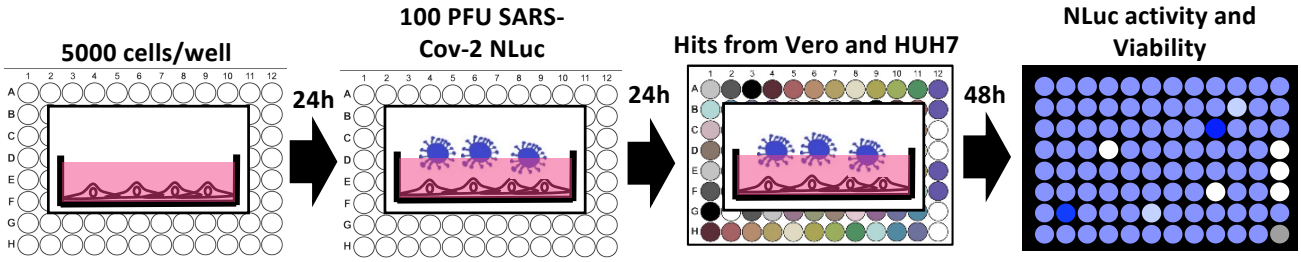

B

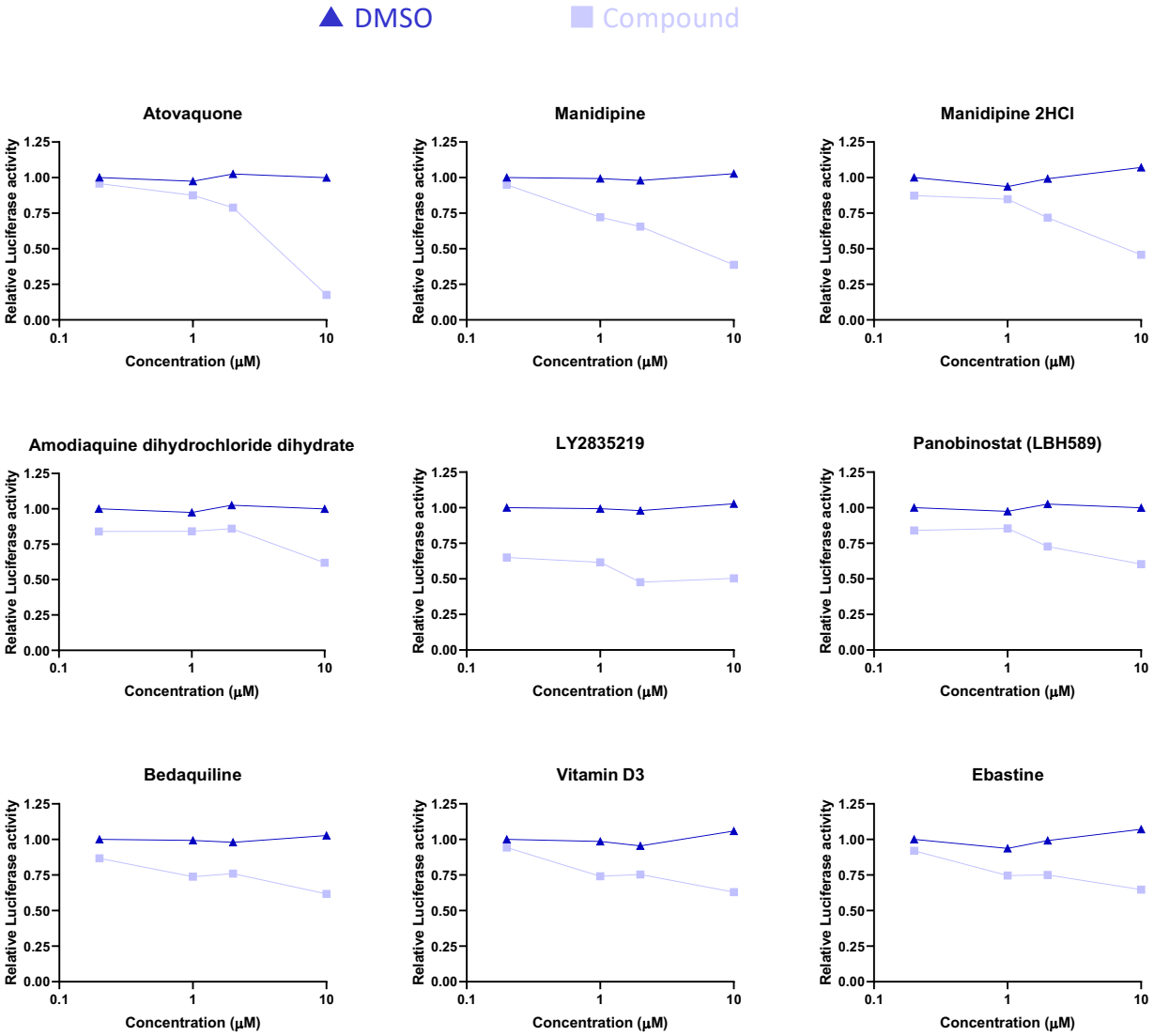

Supplementary Table 1: Source and growth conditions for cell lines used in this study.

Cell line	Growth medium	Source
293T	DMEM + 10% FBS	ATCC
HUH7	DMEM + 10% FBS + NEAA	Accegen #ABC-TC0437
THP1	RPMI + 10%	Sigma-Aldrich, #88081201
SW1353	DMEM + 10% FBS	ATCC® HTB-94™
TC28a	DMEM + 10% FBS	Reference[1]
Hacat	DMEM + 10% FBS	Caltag Medsystems #T0020001
HFF	DMEM + 10% FBS	Cascade Biologics/Thermo Fisher C0045C
Caco2	DMEM + 10% FBS	ECACC #86010202
16HBE14o	AlphaMEM + 10% FBS	Reference [2]
Calu3	AlphaMEM + 10% FBS	ATCC® HTB-55™
A549	DMEM + 10% FBS	ATCC® CCL-185™
HLF (CCD-19Lu)	DMEM + 10% FBS	ATCC® CCL-210™
PodoTERT	PodoUP3	Evercyte #PODO/TERT256
MVGenC	Endothelial Basal medium-2 kit (without VEGF)	NeoBiotech #NB-11-0002
Ab Podocytes	RPMI + 10% FBS + ITS	Reference [3]
HK-2	DMEM:F12 + 10% FBS	ATCC® CRL 2190™
Vero	DMEM + 10% FBS	ATCC® CCL 81™

FBS= Foetal bovine serum, NEAA=Non-essential amino acids, ITS= Insulin-Transferrin-Selenium, VEGF=Vascular endo

References

1 **7989586**
2 **7507342**
3 11856766

thelial growth factor.

Supplementary Table 2: Primers used in this study

Target	Forward	Reverse
Nucleocapsid for RNA generation (P1 and P2)	TACTGTAATACGACTCACTATAGGATGTCTGA TAATGGACCCCAAAATC	TTTTTTTTTTTTTTTTTTTTTTTTTTTTTTTTTTT TTAGGCCTGAGTTGAGTCAGCAC
Sars-Cov2 N	CAACATTGCCAAAAGGCTTC	ACGAGAAGAGGCTTGACTGC
Sars-Cov-2 E	CCATCCTTACTGCGCTTCGA	AAGAAGGTTTTACAAGACTCACGTT
Sars-Cov2 Orf7a	TGGCACTGATAACACTCGCT	TGCCCTCGTATGTTCCAGAAG
NLuc	GACGAGCGCCTGATCAAC	GGTCACTCCGTTGATGGTTAC
ACE2	TTCTGTCACCCGATTTTCAA	TCCCAACAATCGTGAGTGC
TMPRSS2	CGCTGGCCTACTCTGGAA	CTGAGGAGTCGCACTCTATCC
NLP1	TACCCTGAGAATGGGTGGAC	CGTGACAAAGCGCAGAAG
RPLP0	ACTGGTCTAGGACCCGAGAAG	CTCCCACCTTGTCTCCAGTC

Supplemental Table 3: Inhibitors of Sars-Cov2-ΔOrf7a-Nluc replication in Vero cells

Plate	Row	Column	Drug name	Mean relati	SD	PrestoBlue	Replication greater thai
4	A	1	Sitagliptin	0.000141	0.00015	2.560703	1.095235
4	C	1	Belinostat (	0.000366	0.000141	0.89498	1.095828
1	B	10	Cilnidipine	0.00039	0.000274	0.801674	1
9	G	1	Lacidipine	0.000439	0.000302	0.86	1.003471
4	B	1	MK-2048	0.000491	0.000218	2.266647	1.09346
4	H	1	Apixaban	0.00124	0.000138	2.563682	1.098206
4	D	1	LY2784544	0.001449	0.000197	0.785938	1.094642
4	F	1	Rosiglitazo	0.001834	0.000162	3.110979	1.09761
4	G	1	Pioglitazon	0.002045	0.000181	3.48488	1.096421
4	E	1	Lenalidomi	0.002184	0.000236	2.058394	1.094051
9	F	4	Benidipine	0.003673	0.000674	0.808649	1.003968
10	A	5	KPT-330	0.005454	0.002884	0.581033	1.019134
2	A	4	Vortioxetir	0.007391	0.002635	0.508971	1.048162
8	B	2	Fingolimoc	0.007569	0.002924	0.691059	1.112639
12	A	10	Ebastine	0.007931	0.001473	0.605394	1.00847
8	B	3	LY335979 (	0.008621	0.00215	0.586608	1.116935
15	C	1	Atovaquon	0.009591	0.002484	1.549669	1.057471
16	A	2	Eltrombop	0.009908	0.003764	0.719096	1.072602
17	D	5	Bedaquilin	0.010156	0.002018	0.878372	1.050337
17	D	4	Bedaquilin	0.010526	0.001862	1.113109	1.047077
20	A	9	Chlorproth	0.0137	0.002098	0.829945	1.101788
22	A	4	Homoharri	0.014405	0.002412	0.506763	1.060797
1	H	1	Fluoxetine	0.014733	0.000426	0.760391	1.000989
1	H	4	Idarubicin	0.014922	0.000762	0.540586	1.006965
18	A	1	Ospemifen	0.015744	0.004355	0.686275	1.080042
1	H	3	Pamidrona	0.016484	0.000473	0.545607	1.001484
6	A	7	Panobinost	0.018674	0.003673	0.602074	1.07317
3	E	5	Salinomyci	0.018851	0.00162	0.612145	1.043837
16	G	5	Daunorubi	0.021008	0.004246	0.696494	1.089341
14	F	7	Probucol	0.022348	0.00316	0.753645	1.083511
8	F	11	Anidulafun	0.02321	0.002285	0.545309	1.12002
2	G	3	CO-1686 (A	0.023392	0.004377	0.509569	1.075451
10	D	10	Raloxifene	0.026277	0.001894	0.578958	1.018621
1	E	3	Cediranib (	0.026739	0.00104	0.558996	1.022222
1	D	8	LY2835219	0.026845	0.001383	0.551185	1.086418
1	H	2	Epirubicin	0.027999	0.00022	0.912692	1.000494
13	G	1	Cyclosporir	0.031121	0.002339	0.524669	1.087002
9	E	3	Amiodaron	0.03182	0.002961	0.837838	1.007466
6	H	11	Dinaciclib (	0.032924	0.002786	0.663984	1.078891
13	F	3	Chloroxine	0.035536	0.003397	0.577688	1.107189
7	D	1	Isradipine (	0.039218	0.00404	0.615461	1.091102
3	G	5	Vortioxetir	0.042108	0.002727	0.608762	1.090515
5	A	5	Fluvastatin	0.050054	0.005574	0.555306	1.110813
1	C	9	Posaconazo	0.051682	0.00386	0.767643	1.125232
9	D	11	Ciclopirox	0.054363	0.003008	0.517297	1.009476
15	C	10	Doxercalcif	0.055609	0.005686	0.541842	0.544259
9	E	10	Trifluopera	0.056782	0.004016	0.699459	1.01352
4	E	10	Abirateron	0.064772	0.003719	0.564874	1.119405
15	A	1	Tioconazol	0.071615	0.015376	1.172185	0.072057
9	E	7	Nitrendipir	0.072115	0.003323	0.864865	1.012

5	A	7	Lovastatin	0.082796	0.006712	0.547887	0.051421
16	E	5	Paroxetine	0.090967	0.015031	1.087638	0.01146
15	B	1	Vitamin D3	0.096781	0.00863	1.048766	0.001255
13	B	5	Triclabenda	0.09736	0.005545	0.620029	9.97E-06
7	A	9	Duloxetine	0.097981	0.013281	0.991389	1.036885
18	F	9	Amodiaqui	0.100704	0.011124	0.640441	0.002692
16	D	1	Aripiprazol	0.100735	0.013726	0.627768	0.004359
9	F	2	Cabozantin	0.102637	0.003553	0.511892	1.015554
18	A	11	Thonzoniur	0.103504	0.004362	0.604902	3.06E-06
20	C	2	Triclosan	0.106199	0.010286	0.523446	0.001269
9	G	2	Manidipine	0.108566	0.004229	1.035676	1.017085
9	G	3	Manidipine	0.109555	0.003831	0.812973	1.016064
9	F	7	Flunarizine	0.113322	0.008289	2.629189	1.021191
13	E	6	Butoconazo	0.116023	0.007817	0.692194	0.000274
9	F	6	Amlodipine	0.124006	0.008264	1.385405	1.021706
2	C	4	Masitinib (A	0.133853	0.020828	1.308014	0.007066
6	H	1	Clotrimazo	0.138853	0.021956	1.057112	0.00397
17	C	9	Ciclesonide	0.140872	0.016726	0.512541	0.001288
18	B	8	Desogestrel	0.145321	0.013193	0.665686	0.000563

n background q-values

Compound	Reads Counts per second				Relative Recombinant I	% activity in Vero 100PFU screen
(+)-Catechi	362209	357899	366108	367703	0.9620636	160
17-AAG (K	339450	347084	343744	348179	0.912130114	209
Abiraterone	279631	289523	288897	289231	0.759160759	6
Alogliptin B	316906	332493	331161	323679	0.863019788	166
Alosetron H	328498	338671	337783	339698	0.889759897	177
Alvimopan	338215	350063	350082	352328	0.920223412	169
Amiodaron	364410	365102	365644	366409	0.967122986	5
Amodiaqui	351271	347518	344113	339282	0.914596284	12
AN-2690	329173	329953	332892	324160	0.870919869	171
Anidulafun	365229	376574	364202	366012	0.974039114	5
Ascomycin	312887	325360	316950	314498	0.840161895	171
AT13387	289397	302902	309451	303901	0.797783743	191
Atovaquon	224278	226697	224646	216287	0.590178835	4
Baicalin	353023	358945	357158	357276	0.943855499	164
Baricitinib p	337511	341167	346435	349331	0.909474697	199
Bedaquilin	348601	355872	347079	351646	0.928501326	4
Bedaquilin	351974	352561	351293	338630	0.922718035	4
Belinostat	351877	362403	352055	355423	0.940782547	5
Benidipine	50508	49563	49185	49177	0.131303853	2
Bivalirudin	309590	311058	307409	301908	0.813872407	172
Boceprevir	341877	348889	346623	349417	0.917654679	178
Cabozantir	333265	320522	329153	328687	0.867908455	12
Caffeic acid	390077	320522	399891	403178	1.053990126	173
Cediranib (	350524	320522	354116	362844	0.943901818	3
Cetirizine	170134	320522	168670	171706	0.448561006	161
Chloroxine	380665	320522	374596	374884	0.997545476	6
Chlorprothi	359664	320522	361391	361186	0.957434982	4
Ciclopirox e	358391	320522	365653	361119	0.961032665	7
Cilnidipine	28828	320522	28106	27971	0.075210567	1
CO-1686 (A	327566	320522	324163	319872	0.855087284	3
Cyclosporir	373363	320522	381885	373048	1.000139355	6
Daidzein	339091	320522	350216	346126	0.915372462	161
Daunorubic	319222	320522	327409	328432	0.86150581	5
Dinaciclib (S	345056	320522	342151	346073	0.913362207	5
Doxercalcif	361602	320522	370984	356613	0.961268894	8
Duloxetine	297459	320522	293652	301826	0.789374812	12
Ebastine	323732	320522	324560	326603	0.857585216	4
Eltrombopa	331875	320522	331553	322913	0.866618795	4
Epirubicin H	298948	320522	302560	310338	0.802456032	3
Ethamsylat	388357	320522	391647	386776	1.028650844	167
Fingolimod	354171	320522	356587	351555	0.939334077	3
Fluoxetine	317425	320522	314163	307707	0.830595645	2
Fluvastatin	344916	320522	339204	335899	0.899431358	6
Idarubicin H	327538	320522	325691	318222	0.860993651	2
Isradipine (	19176	320522	18561	18431	0.049588738	6
KPT-330	378225	320522	389989	381493	1.021585172	4
Lacidipine	61246	320522	60310	59492	0.160064805	1
Levodopa	304150	320522	322065	316577	0.839019133	233
L-Glutamin	349150	320522	361792	350740	0.941896194	204

Lithium Citr	343238	320522	350985	343490	0.921697688	205
Lithocholic	350340	320522	350189	353302	0.934238297	205
Lovastatin	351803	320522	353101	349914	0.931862781	9
LY283521	345999	320522	345910	348685	0.918872213	3
LY335979	352212	320522	356783	351420	0.936199587	3
Manidipine	249924	320522	250350	251205	0.661459544	12
Manidipine	242466	320522	242968	239469	0.638229111	12
Meloxicam	308460	320522	309204	312953	0.824020956	178
Mepenzola	330221	320522	339233	336213	0.889583222	175
Methyldopa	361429	320522	364798	367357	0.966613475	175
NAD+	385544	320522	386401	376264	1.016345802	164
Nevirapine	371882	320522	379254	373316	0.993240432	187
Nitrendipin	26271	320522	26096	26141	0.069146715	9
Noscapine	358232	320522	362883	354994	0.950175431	213
Ospemifen	356755	320522	358779	352991	0.940726302	4
Oxethazair	330534	320522	331517	321724	0.873612341	167
Pamidrona	309519	320522	313471	313941	0.831273891	2
Panobinos	330994	320522	343634	341728	0.896255842	4
Paroxetine	360169	320522	369849	368856	0.973172282	12
Posaconaz	325406	320522	324458	315077	0.856451055	6
Probucol	337686	320522	341300	339611	0.902269406	5
Raloxifene	334037	320522	331016	335545	0.88121267	6
Ranolazine	359507	320522	367539	367791	0.967918354	167
Ruxolitinib	314540	320522	317488	316727	0.838138405	169
Salinomycii	365050	320522	373342	367850	0.977863099	4
Tioconazol	349867	320522	345556	349383	0.922076183	10
Triclabenda	335937	320522	336143	339544	0.892308118	12
Trifluopera	358281	320522	348422	360671	0.939701323	7
Vitamin D3	370629	320522	360711	364312	0.968153921	12
Vortioxetin	326546	320522	329264	332965	0.87317297	6
Vortioxetin	280784	320522	284246	284019	0.747903855	1
DMSO	356875	320522	360022	355819	0.945032008	100
DMSO1	365885	320522	366954	370334	0.969202059	100
DMSO2	387195	320522	397670	396896	1.042738516	100
DMSO3	382401	320522	382402	379669	1.012664744	100
DMSO4	390492	320522	388004	391251	1.030362672	100

Compounds that inhibited SARS-Cov2-ΔOrf7a-Nluc replication in Vero and HUH7 screens

HUH7	Row	Column	Drug name	Mean relati	SD	PrestoBlue
9	E	3	Amiodarone HCl	0.034035	0.002111	0.963298
9	F	6	Amlodipine Besylate	0.033811	0.002081	0.68594
18	F	9	Amodiaquine dihydrochlorid	0.012584	0.000224	0.778309
16	D	1	Aripiprazole	0.008694	0.001695	0.741567
15	C	1	Atovaquone	0.058244	0.010118	1.150489
17	D	4	Bedaquiline fumarate	0.108424	0.006709	0.522411
9	*F*	*4*	*Benidipine HCl*	*0.00382*	*0.0012*	*0.66087*
9	F	2	Cabozantinib malate (XL184)	0.03412	0.003109	0.801129
20	A	9	Chlorprothixene (hydrochlori	0.031761	0.003566	0.762326
9	D	11	Ciclopirox ethanolamine	0.046013	0.000597	0.502315
1	*B*	*10*	*Cilnidipine*	*0.00182*	*0.00039*	*0.79704*
13	G	1	Cyclosporin A	0.080205	0.007228	0.506995
16	G	5	Daunorubicin HCl	0.006058	0.001727	0.518582
6	H	11	Dinaciclib (SCH727965)	0.062944	0.000228	0.593445
7	A	9	Duloxetine HCl	0.028451	0.00042	0.504807
12	A	10	Ebastine	0.015939	0.00032	1.613674
9	F	7	Flunarizine 2HCl	0.109125	0.006023	0.968944
1	H	1	Fluoxetine HCl	0.080571	0.001764	0.91596
5	A	5	Fluvastatin Sodium	0.05448	0.002919	1.301701
22	A	4	Homoharringtonine	0.013304	0.003262	0.679424
7	*D*	*1*	*Isradipine (Dynacirc)*	*0.00135*	*0.00094*	*0.67618*
10	A	5	KPT-330	0.058589	0.000707	0.710223
9	*G*	*1*	*Lacidipine*	*0.02662*	*0.00129*	*0.92468*
5	A	7	Lovastatin	0.087582	0.002308	1.075407
1	D	8	LY2835219	0.072422	0.002963	0.604272
8	B	3	LY335979 (Zosuquidar 3HCL)	0.082311	0.009091	0.620331
9	G	2	Manidipine	0.100031	0.002327	0.539582
9	G	3	Manidipine 2HCl	0.044466	0.002178	0.572558
2	C	4	Masitinib (AB1010)	0.039172	0.000431	0.715617
9	*E*	*7*	*Nitrendipine*	*0.00073*	*0.00059*	*0.65455*
18	A	1	Ospemifene	0.144859	0.002836	1.203434
6	A	7	Panobinostat (LBH589)	0.058971	0.000949	0.753019
10	D	10	Raloxifene HCl	0.036459	0.000553	0.5413
15	A	1	Tioconazole	0.124683	0.020143	1.128639
15	B	1	Vitamin D3	0.025671	0.009357	0.641766

Red indicates Nluc inhibitors